Development of an ^{18}F-labelled irreversible inhibitor of transglutaminase 2 as radiometric tool for quantitative expression profiling in cells and tissues

Wodtke, R.; Wodtke, J.; Hauser, S.; Laube, M.; Bauer, D.; Rothe, R.; Neuber, C.; Pietsch, M.; Kopka, K.; Pietzsch, J.; Löser, R.;

Originally published:

March 2021

Journal of Medicinal Chemistry 64(2021)6, 3462-3478

DOI: https://doi.org/10.1021/acs.jmedchem.1c00096

Development of an ^{18}F-labelled irreversible inhibitor of transglutaminase 2 as radiometric tool for quantitative expression profiling in cells and tissues

Robert Wodtke[a*], Johanna Wodtke[a], Sandra Hauser,[a] Markus Laube[a], David Bauer[a,c], Rebecca Rothe[a,c], Christin Neuber[a], Markus Pietsch[b], Klaus Kopka[a,c], Jens Pietzsch[a,c], Reik Löser[a,c,*]

[a] Helmholtz-Zentrum Dresden-Rossendorf, Institut für Radiopharmazeutische Krebsforschung, Bautzner Landstraße 400, 01328 Dresden, Germany

[b] Institut II für Pharmakologie, Zentrum für Pharmakologie, Medizinische Fakultät, Universität zu Köln, Gleueler Straße 24, 50931 Köln, Germany

[c] Fakultät Chemie und Lebensmittelchemie, Technische Universität Dresden, Mommsenstraße 4, 01062 Dresden, Germany

Abstract:

The transamidase activity of transglutaminase 2 (TGase 2) is considered to be important for several pathophysiological processes including fibrotic and neoplastic tissue growth, whereas in healthy cells this enzymatic function is predominantly latent. Methods that enable the highly sensitive detection of TGase 2, such as application of radiolabelled activity-based probes, will support the exploration of the enzyme's function in various diseases. In this context, the radiosynthesis and detailed *in vitro* radiopharmacological evaluation of an ^{18}F-labelled N^{ε}-acryloyllysine piperazide is reported. Robust and facile detection of the radiotracer-TGase 2 complex by autoradiography of thin layer plates and polyacrylamide gels after chromatographic and electrophoretic separation owing to irreversible covalent bond formation was demonstrated for the isolated protein, cell lysates and living cells. Using this radiotracer, quantitative data on the expression profile of activatable TGase 2 in mouse organs and selected tumours were obtained for the first time by autoradiography of tissue sections.

Introduction

Activity-based probes offer great potential for advancing the biological understanding of enzymes in their native cellular contexts.[1, 2] Their general structure is characterised by combining reactive moieties for stable covalent targeting with recognition elements that confer selectivity by engaging in non-covalent interactions with the target enzyme/protein, which are complemented by a reporter tag that accounts for reliable and sensitive detection after binding to the protein of interest.[3, 4] Concerning the formation of stable covalent bonds between the probe molecule and the protein of interest, enzymes that form covalent intermediates with nucleophilic residues such as serine, cysteine, lysine and aspartic acid residues during catalysis are particularly amenable for targeting with activity-based probes.[5] Nevertheless, also enzymes that do not rely on such intermediates and even proteins without catalytic activity can potentially be monitored in this way by targeting non-catalytic nucleophilic residues in these proteins.[6, 7] However, the most straight-forward approach for the design of activity-based probes is based on irreversible enzyme inhibitors containing electrophilic warheads which are capable of stable and selective covalent bonding to nucleophilic residues in the enzyme's active site.[8, 9] The reporter tag, however, should preferably not compromise the inhibitory activity, the selectivity profile and the membrane permeability of the original inhibitor molecule.[10] Very often, fluorophores and affinity handles, e.g. biotin, have been employed as reporter tags. Given their considerable steric demand and the requirements mentioned before, the reporter groups are often attached after incubation of the sample with the probe molecule by bioorthogonal reactions such as copper-catalysed azide-alkyne cycloaddition subsequent to cell lysis.[11, 12]

Reporter groups that overcome these shortcomings can be obtained by labelling with radionuclides as the ionising radiation that is emitted during their transformation into stable nuclides can be detected in a highly sensitive manner, which even allows their use in sub-

stoichiometric amounts in accordance with de Hevesy's radiotracer principle. Therefore, the biochemical process under investigation, will not be influenced by the presence of the probe molecule.[13] Furthermore, considering that the radiolabel will consist of only one atom, the molecular properties of the original inhibitor will only be minimally influenced, provided that the radionuclide can be covalently attached to the molecule. Despite these advantages, radiolabelled activity-based probes are only scarcely reported. The few examples include diisopropylfluorophosphate labelled with tritium[14] or phosphorus-32 [15] and ^{3}H-labelled lactacystin[16] for the detection of acetylcholine esterase and 20S proteasomes, respectively. Penicillin derivatives labelled with carbon-14[17], tritium[18] and iodine-125[19] were used to detect penicillin-binding proteins involved in cell wall biosynthesis in *Staphylococcus aureus*. Furthermore, papain-like cysteine cathepsins and de-ubiquitinating enzymes were probed with E64-derivatives[20, 21] and ubiquitin vinylsulfone,[22] respectively, each labelled with iodine-125.

An enzyme that is in the focus of our research is transglutaminase 2 (TGase 2), because of its important functions in tumour progression and cell survival, which are increasingly recognized.[23] In addition, it has an important function in mediating cell-matrix interactions.[24] Moreover, apart from neoplastic malignancies, the enzyme is involved in the pathogenesis of several other diseases,[25] of which celiac disease is the most prominent example.[26, 27] TGase 2 represents a multifunctional protein that is composed of four domains. Its two main functions, the eponymous acyl transferase and G-protein activities are associated with two inversely regulated conformational states, which are the open and closed conformations, respectively. In addition, TGase 2 can interact with numerous other proteins both in the intra- and extracellular domain, such as fibronectin, integrin and syndecan-4.[28] Therefore, binding activities that are associated with both conformational states and acyltransferase/transamidase activity, which is ascribed exclusively to the open conformation, should be considered separately.[29] Hence, the development of activity-based probes for this enzyme appears to be a worthwhile endeavour.[30, 31] The catalytic site responsible for the acyl

transferase activity of TGase 2 is constituted by the residues Cys 277, His 335 and Asp 358 (numbering according to the human enzyme), which are harbored by the central α/β domain. Mechanistically, a thiol ester intermediate is initially formed between the Gln side chain of the acyl donor substrate and Cys 277, which can undergo deacylation by various nucleophiles, predominantly primary amines such as lysine residues and low-molecular weight biogenic amines.[32] For irreversible inhibition of the acyl transferase activity by targeting the active site residue Cys 277 covalently, *N*$^{\varepsilon}$-acryloyllysine derivatives appear highly attractive as they exhibit a high inhibitory potency and selectivity.[33-36] Therefore, such compounds represent a viable basis for the design of activity-based TGase 2 probes. Radiotracers derived from *N*$^{\varepsilon}$-acryloyllysines will allow for selective detection of the acyl transferase activity at the cellular level and are highly desirable because the biological significance of this function in the context of disease progression is still not completely understood.[29] Furthermore, as the transamidase function can be induced in the presence of Ca^{2+}, such probes would enable the convenient and quantitative measurement of TGase 2 expression levels in vitro. In addition, activity-based probes potentially enable the assessment of target occupancy under therapeutic inhibitor treatment,[37, 38] which would support drug discovery for TGase 2.

Next to the radionuclides mentioned before, labelling of activity-based probes with fluorine-18 appears to be particularly attractive as it potentially allows the detection of the enzyme-inhibitor complex and hence target occupancy studies in vivo by quantitative imaging using positron emission tomography (PET), provided that the compound exhibits a sufficient pharmacokinetic performance in terms of metabolic stability and circulation time.[38] This is due to the almost optimal physical properties of this radionuclide, which undergoes nuclear transformation into oxygen-18 yielding positrons of 634 keV (E_{max}) with a branching ratio of 97%. As these particles each undergo conversion into two γ photons of 511 keV upon annihilation with an electron, fluorine-18 can be detected with high sensitivity and spatial resolution.[39] Furthermore, from a chemical point of view, the extraordinarily stable carbon-fluorine bond accounts for a usually

very robust covalent attachment of the radiolabel.[40, 41] In addition to these advantages, its rather short half-life of 109.8 min renders this radionuclide favourable concerning aspects of radiation protection, also with regards to in vitro applications.

We recently published a study on the structure-activity relationships of N^{ε}-acryloyllysine piperazide-derived TGase 2 inhibitors with a special emphasis on fluorinated derivatives. This included also the consideration of selectivity towards other isoenzymes of the transglutaminase family and in vitro pharmacokinetic parameters such as membrane permeability coefficients.[36] Within this study, several radiotracer candidates for labelling with fluorine-18 were identified. The most promising compound considering both pharmacological properties and the feasibility of ^{18}F-fluorination appeared to be **7b** (Figure 1). Besides this study, reports on other radiotracers were published in the context of TGase 2 research (Figure 1). [1-^{14}C]Iodoacetamide was used to demonstrate the importance of Cys 277 as an active site residue in guinea pig TGase 2.[42] Much more recently, ^{11}C-labelled inhibitors of the acrylamide chemotype such as [^{11}C]**A**[43] and the ^{18}F-labelled peptidic diazomethyl ketone [^{18}F]**B**[44] were published. These radiotracers were mainly evaluated for PET imaging *in vivo* using a tumour xenograft model,[45] whereas targeting of TGase 2 at the molecular level based on the detection of the radiolabelled TGase 2-inhibitor complex was not demonstrated in these studies.

Considering the compelling evidence that TGase 2 is important in several human disease states, including cancer, quantitative detection of this enzyme in complex biological samples by activity-based probes has not been reported so far. Therefore, the objective of this work was to label the pre-evaluated irreversible fluorinated inhibitor **7b** of TGase 2 with fluorine-18 by establishing an optimised radiochemical methodology and application of the resulting radiotracer [^{18}F]**7b** for the sensitive and quantitative detection of TGase 2 at the molecular, cellular and organ level is reported.

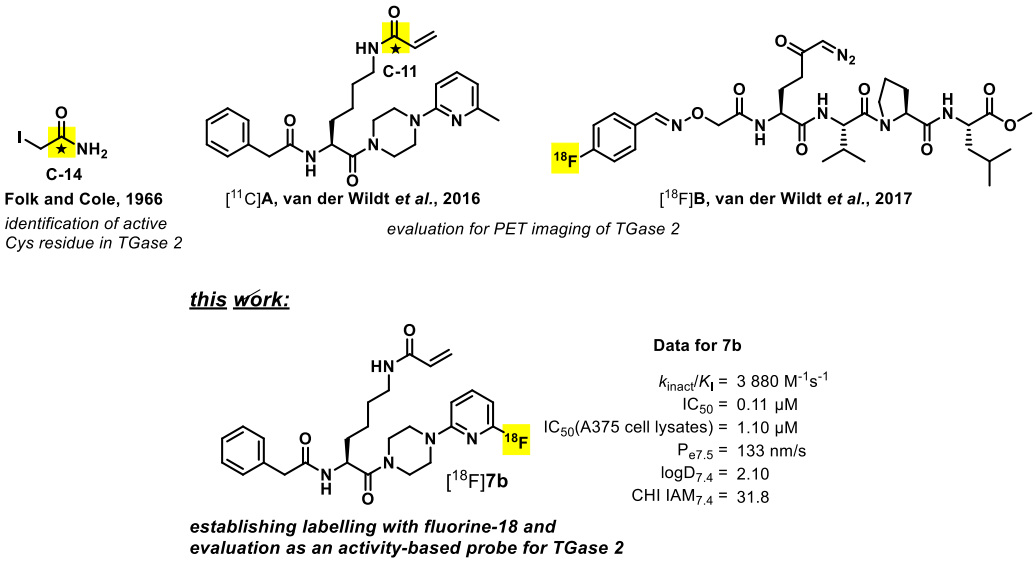

Figure 1. Structures of previously reported TGase 2-directed radiotracers and [^{18}F]7b

---

All data for **7b** have been previously reported (same numbering in ref. [36]).

Results and Discussion

Synthesis of precursors and labelling with fluorine-18

Radiosynthesis of [^{18}F]**7b** was envisaged by reacting the corresponding nitro-substituted compound **7a** with [^{18}F]fluoride. The synthesis of precursor and reference compounds was performed as recently described by us (Scheme 1).[36] In brief, the respective pyridylpiperazines **4a** and **4b** were obtained via Buchwald-Hartwig amination and nucleophilic aromatic substitution, respectively, and subsequent Boc removal using TFA/CH_2Cl_2. N^{α}-Boc-N^{ε}-acryloyl-L-lysine (**3**) was prepared by N^{ε}-acryloylation of commercially available Boc-L-lysine. Then, coupling of the building blocks was achieved under common conditions for amide bond formation (PyBOP as coupling agent and DIPEA as base) to provide compounds **5**. Subsequently, the Boc group was removed by treatment with TFA/CH_2Cl_2 (compounds **6**) and final acylation yielded precursor **7a** and reference compound **7b**.

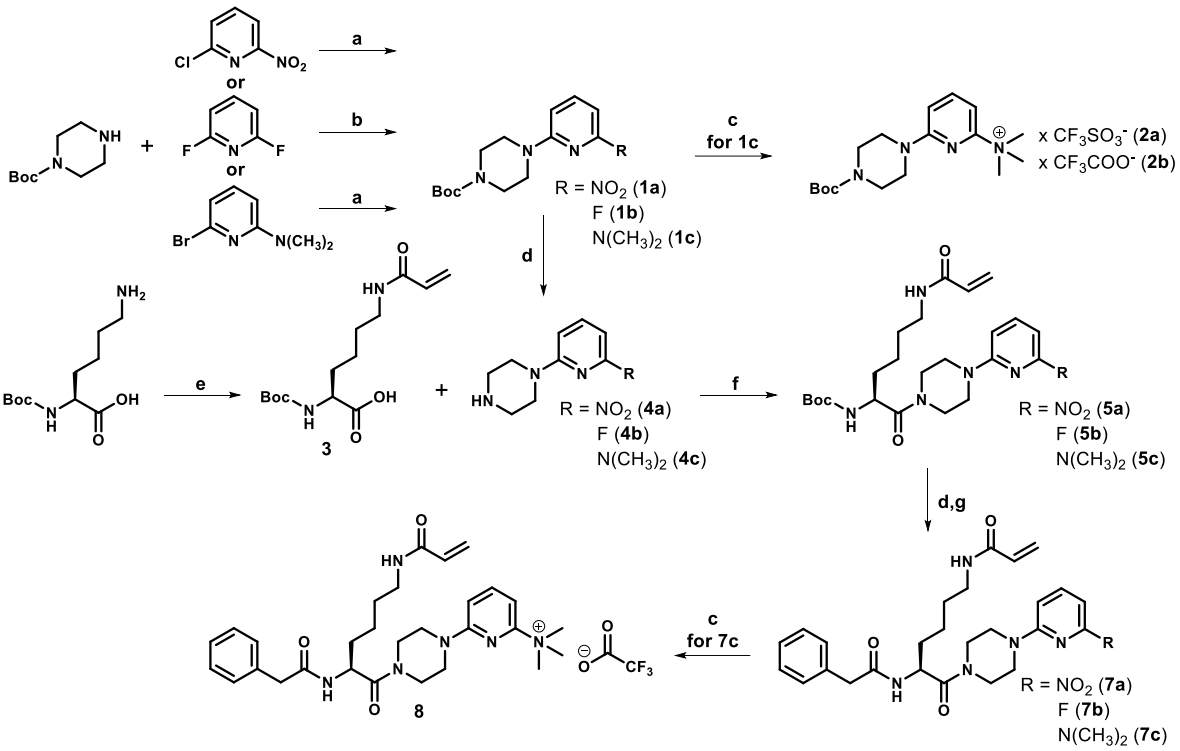

Scheme 1. Synthesis steps to precursors and reference compounds

---

Reagents and conditions: **a)** Cs_2CO_3, Xantphos, $Pd_2(dba)_3$, THF, Ar, 70°C, 12 h; **b)** TEA, DMF, 150°C, 24 h; **c)** methyl triflate, CH_2Cl_2, 17 h; **d)** TFA/CH_2Cl_2 (1/1), 2 h; **e)** *N*-acryloxysuccinimide, TEA, CH_3OH, 2 h; **f)** PyBOP, DIPEA, THF, 5 h; **g)** phenylacetyl chloride, TEA, CH_2Cl_2, 5 h. Facing the slightly unsatisfying yields en route to **8**, an alternative synthetic path starting from Fmoc-Lys(Boc)-OH was attempted (see Scheme S1 in Supporting Information), which, however, did not result in improved yields.

The ^{18}F-labelling of **7a** (and also the structurally less complex nitropyridine **1a**) did not lead to satisfying labelling yields (RCC≈20%, determined by radio-TLC) accompanied by the formation of base-induced side products and a challenging chromatographic separation of **7a** from [^{18}F]**7b** (a detailed discussion on these experiments can be found within the Supporting Information, Discussion S1). Therefore, the trimethylammonio-substituted analogue of **7a**, i.e. **8**, was envisaged as alternative precursor compound, which in particular enables radiofluorinations with alternative conditioning of [^{18}F]fluoride via ion pair formation in methanol ("minimalist" approach).[46] To afford precursor **8**, building block **1c** was required, which was obtained by reacting 6-bromo-2-*N*,*N*-dimethylaminopyridine with Boc-piperazine under

Buchwald-Hartwig conditions.[47] The remaining steps resemble those of the synthesis of **7a** (Scheme 1), apart from the last step, which was the formation of the trimethylammonio group by reaction with methyl triflate. This step proved to be critical as the corresponding ring-methylated compound (**11**, see Supporting Information) was obtained in addition to the desired quarternary pyridylamine **8**, which is interpreted as intermolecular transmethylation rather than intramolecular methyl migration. Therefore, purification had to be performed by preparative RP-HPLC providing **8** as trifluoroacetate salt. As in the ^{18}F-denitrofluorination approach, radiofluorination was attempted with the structurally less complex trimethylammonio-substituted Boc-pyridylpiperazine **2a** (triflate salt) as precursor. This compound was obtained by reaction of the dimethylamino-substituted building block **1c** with methyl triflate. Even though performed as for compound **8**, quaternisation of the dimethylamino group in **1c** proved to be less cumbersome as it was possible to isolate the corresponding trimethylammonium triflate **2a** by precipitation and the formation of the side product methylated at the ring nitrogen atom was not noticed. Compound **2b** (trifluoroacetate salt) was obtained from **2a** by repetitive lyophilisations of a solution of **2a** in 0.1% TFA/water.

Radiofluorination of the trimethylammonio pyridines **2a** and **2b** resulted in high radiochemical conversions (RCC>70%, determined by radio-TLC, Table S1 in Supporting Information) independent of using classical conditions for azeotropic drying of [^{18}F]fluoride (K_2CO_3/K_{222}) or the “minimalist” approach[46] without the addition of base and cryptand.

Favourably, similar radiochemical conversion using the “minimalist” approach were observed for radiofluorination of the *N*$^{\varepsilon}$-acryloyllysine-derived precursor **8** to the desired radiotracer [^{18}F]**7b** (Figure 2A). In contrast to radiolabelling of precursor **7a**, the radio-HPLC profile showed no significant radiolabelled side products for the corresponding trimethylammonium precursor (Figure 2B). This indicates that both changing the leaving group and the absence of base are advantageous for the radiofluorination reaction. However, in the UV detector trace, two peaks were observed in addition to that of remaining precursor **8**, which were assigned to the

corresponding dimethylamino- and methoxy-substituted compounds **7c** and **7d**, respectively, on the basis of mass-spectrometric analysis. The non-radioactive side product **7d** arises from the reaction of **8** with residual methanol that remains from the elution of [^{18}F]fluoride as competing nucleophilic aromatic substitution. On the other hand, the trimethylammonio group of **8** is prone to S_N2 reaction with present nucleophiles at its methyl groups, which leads to **7c**, probably due to attack of the trifluoroacetate anion, which is present in excess over [^{18}F]fluoride in the reaction mixture. The formation of these non-radioactive side products did not impede the purification of [^{18}F]**7b** by semi-preparative HPLC, which resulted in high chemical purities, as indicated by the absence of peaks apart of that for **7b** in the UV detector trace and radiochemical purities >97% as determined by analytical radio-HPLC (Figure 2C) and also radio-TLC (Figure S3 in Supporting Information). On the basis of precursor **8**, a reliable radiosynthesis (n=22, synthesis time <90 min) of the TGase 2-targeting radiotracer [^{18}F]**7b** in good isolated radiochemical yields (33±14% based on [^{18}F]F^- eluted from the cartridge) and moderate to good molar activities (9-213 GBq/µmol) was established, which enabled its subsequent radiopharmacological evaluation.

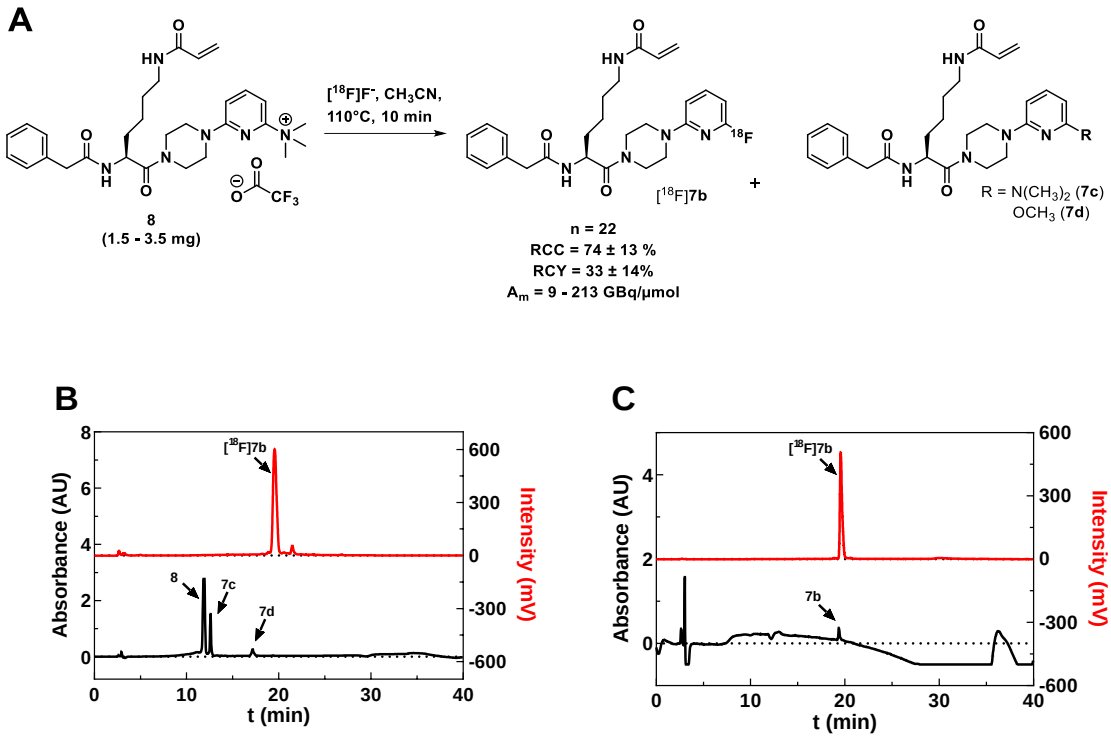

Figure 2. Products from ^{18}F-labelling of trimethylammoniopyridine precursor 8

A) Structures of products and results for ^{18}F-labelling of precursor **8** under the given reaction conditions. RCC determined by radio-TLC. RCY (isolated) based on [^{18}F]F$^-$ eluted from the cartridge. **B**-**C)** RP-HPLC analysis of the crude mixture for ^{18}F-labelling of **8** (**B**) and for [^{18}F]**7b** after RP-HPLC purification (**C**). UV(220 nm for **B**; 214 nm for **C**)- and radioactivity-detection chromatograms are shown in black and red, respectively. For RP-HPLC conditions see Experimental Section.

As precursor compounds **7c** and **8** potentially represent potent irreversible inhibitors of TGase 2, their inhibitory potency towards human (h) TGase 2 was determined by using an in-house fluorescence polarisation assay recently described by our group.[36, 48] IC_{50} values (mean±SEM) at pH 8.0 of 0.25 (±0.04) and 0.34 (±0.10) µM were obtained for **7c** and **8**, respectively. Therefore, the dimethylamino and trimethylammonio groups were similarly tolerated as the methyl group (compound **A** in Figure S6 in Supporting Information, IC_{50} = 0.31 µM) of the lead compound in our previous study on structure-activity relationships at the *N*$^{\varepsilon}$-acryloyllysine scaffold.[34, 36] This result is not suprising as even more sterically demanding

groups in position 6 of the pyridine ring are well tolerated or lead to even higher inhibitory potencies.[36]

Radiopharmacological characterisation of [^{18}F]7b in vitro

*Stability of [^{18}F]**7b** in various media and determination of log$D_{7.4}$*

Initially, the stability of [^{18}F]**7b** was evaluated in aqueous media in the absence and presence of glutathione. As indicated by the γ-detected chromatograms in Figure S4 in the Supporting Information, virtually no chemical change is detectable in PBS at 37 °C after 4 h, whereas some additional peaks are visible after 3 h in the presence of 1 mM glutathione even though their area is negligible in relation to the original compound. This result is in agreement with other studies that indicate that aliphatic acrylamides are sufficiently stable concerning their reaction with biogenic thiols.[49, 50] As the radiotracer is stored in ethanolic solution during the period of experimentation, its stability was also investigated in this medium. No significant changes were visible in the chromatograms obtained after 1.5 h, 5 h and 7 h of storage at room temperature (Figure S4). Furthermore, [^{18}F]**7b** exhibits also an excellent stability in cell culture supernant (DMEM medium) for a sufficient time, exemplarily shown for A375hS100A4 cells (Figure S4). The log$D_{7.4}$ value of [^{18}F]**7b** was determined to be 2.1 by using the classic shaking flask method and an HPLC-based method. The obtained values are in excellent agreement with the previously determined log$D_{7.4}$ value of **7b** by ^{19}F-NMR spectroscopy (2.1)[36] and highlights the reliability of these methods for the determination of this physicochemical parameter.

*Radio-TLC[51] binding experiments of [^{18}F]**7b** with recombinant hTGase 2*

The stability of radiotracer [^{18}F]**7b** in protic media encouraged the investigation of its target binding, which was accomplished by taking advantage of the irreversible interaction of acrylamide-based inhibitors with transglutaminases. The robust covalent enzyme-inhibitor

complex should allow for the facile separation of enzyme-bound and free radiotracer by simple radio-TLC on silica adsorbent and both radioactive species could be easily quantified by radioluminographic detection followed by densitometric analysis. Therefore, this method should allow for the determination of this salient kinetic parameter by direct monitoring of the enzyme-inhibitor complex, which otherwise can only be obtained indirectly by monitoring and analysing substrate conversion.[52, 53] Furthermore, the fact that radiolabelled inhibitor [^{18}F]**7b** can be detected in low amounts enables application of the enzyme in large excess over the inhibitor, which allows for consideration of both monitoring the increase of the enzyme-radiotracer complex and the decrease of free radiotracer. The results of the radio-TLC experiment are shown in Figure 3. The progress curves (decrease of free radiotracer) were analysed by nonlinear regression using one-phase decay and the obtained rate constant k_{obs} is equal to k_{inact}*[E]/K_I for the present conditions (see Figure S5 in Supporting Information for a detailed explanation). Division by [E] yields the second-order inactivation constant k_{inact}/K_I. Worth of note, the determined k_{inact}/K_I value of 4 070 $M^{-1}s^{-1}$ for [^{18}F]**7b** towards hTGase 2 at pH 6.5 is in good agreement with the value of **7b** determined in the fluorimetric enzyme assay at the same pH value (3 850 $M^{-1}s^{-1}$).[36] Interestingly, the rate constant for the formation of the hTGase 2-[^{18}F]**7b** complex is twice as high at pH 7.4 and even higher at pH 8.0 compared to pH 6.5. Determination of the value for **7b** under classical conditions in the fluorimetric assay was not possible at pH values higher than pH 6.5 due to the pronounced spontaneous hydrolysis of the fluorogenic substrate.[54] Exemplarily, we also demonstrated the selectivity of [^{18}F]**7b** towards hTGase 2 by testing the kinetics of its interaction with hTGase 6, which is the one of the eight human TGase isoenzymes most closely related to TGase 2 [36, 55]. As shown in Figures 4B and C, the enzyme-inhibitor complex is formed very slowly with a k_{inact}/K_I of 7 $M^{-1}s^{-1}$, which is more than 500fold less than the respective value for TGase 2. This indicates the excellent selectivity of [^{18}F]**7b**.

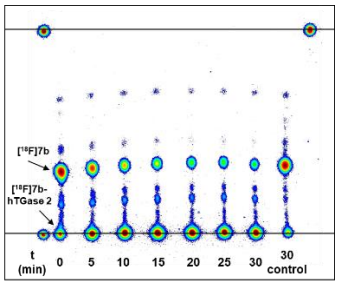

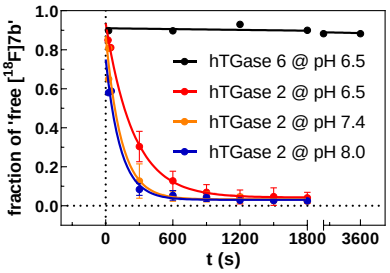

	pH	k_{inact}/K_I ($M^{-1}s^{-1}$)
hTGase 2	6.5	4,070 (590)
	7.4	7,900 (2,630)
	8.0	9,080 (830)
hTGase 6	6.5	7

Figure 3. Radio-TLC experiments for determining the inhibitory activity and selectivity of [^{18}F]7b towards hTGase 2

Left: Radio-TLC for the reaction of [^{18}F]**7b** with hTGase 2 analysed at the given time points. Spots are shown in rainbow colours. [^{18}F]**7b** exhibits an R_f value of around 0.3 and the complex [^{18}F]**7b**-hTGase 2 does not move away from the starting spot. Stationary phase: silica gel, mobile phase: ethyl acetate (two runs). For lane '30 min control', hTGase 2 was omitted in the reaction mixture. **Middle:** Plots of (fraction of 'free [^{18}F]**7b**'=f(t) for hTGase 2 and hTGase 6 at the given pH values including non-linear regressions according to one-phase decay. The fraction of free [^{18}F]**7b** was obtained by integration of the radio-TLC spots for 'free [^{18}F]**7b**' and the complex '[^{18}F]**7b**-hTGase 2'. **Right:** Summary of k_{inact}/K_I values derived from non-linear regressions. Data shown are values of one or two (mean ± SD) experiments. For further details see Experimental Section. Conditions: 30 °C, 3 mM $CaCl_2$, 1 mM TCEP, 0.1 mg/mL (1.3 µM) hTGase 2 or 0.05 mg/mL hTGase 6.

The proven validity of this method encouraged us to investigate the influence of Ca^{2+} concentration on radiotracer binding (Figure 4A). From this experiment an EC_{50} value for the effective calcium concentration of 0.19 mM and a Hill coefficient of 5.7 were obtained. The obtained EC_{50} confirms previously reported values determined on human TGase 2 with fluorescence-based methods.[56, 57] Furthermore, the Hill coefficient is in good agreement to results from equilibrium dialysis demonstrating that up to six Ca^{2+} (at five Ca^{2+}-binding sites) can bind to the hTGase 2 protein.[58, 59] As mentioned above, the transamidase activity is associated with the open conformation of TGase 2, which is stabilised by occupation of the calcium binding sites. The observed calcium dependency of radiotracer binding therefore demonstrates that [^{18}F]**7b** very sensitively detects the open conformation. Binding of [^{18}F]**7b** to

TGase 2 was furthermore investigated at a sub-effective Ca^{2+} concentration of 0.1 mM, where radiotracer binding at 30 min is almost negligible. However, for prolonged time of incubation (up to 4 h), radiotracer binding significantly increases over the period of observation (Figure 4B). Like transamidation substrates, acyltransferase domain-directed inhibitors of TGase 2 can only bind to the open conformation of the enzyme, which predominates only at higher calcium concentrations.[60] However, even under conditions in which the closed conformation is mainly adopted, i.e. at low calcium concentrations and in the presence of purine nucleotides, acyltransferase-site directed irreversible inhibitors should be able to bind to TGase 2 if sufficient time is provided. Time-dependent binding of [^{18}F]**7b** to TGase 2 under conditions in which the enzyme is present in large excess over the inhibitor confirms that a dynamic equilibrium exists between the open and closed conformation, as concluded from other studies, even though the influence from inhibitor binding itself on the equilibrium could not be excluded in these investigations.[60-62]

Further binding experiments of [^{18}F]**7b** to hTGase 2 were performed in the presence of GTP-γ-S, a non-hydrolysable GTP analogue. GTP (and further purine nucleotides such as GDP and ATP) allosterically inhibit the transamidase activity by forcing TGase 2 to adopt the closed conformation.[63, 64] To facilitate binding of GTP-γ-S, the Ca^{2+} concentration was adjusted to 0.2 mM, which is near the EC_{50} value for Ca^{2+} binding (Figure 4A). As shown in Figure 4C, binding of [^{18}F]**7b** to hTGase 2 was decreased with increasing concentration of GTP-γ-S and nonlinear regression revealed an IC_{50} value of 710 nM for this nucleotide analogue. This value is lower than the determined IC_{50} value of 5 µM by Schaertl et al. who used a fluorescent transamidation assay (substrates pair *N*,*N*,dimethylcasein and KxD).[65] However, the Ca^{2+} concentration in this assay was 0.5 instead of 0.2 mM employed herein, which might explain the difference.

In addition to the characterisation of GTP analogues, [^{18}F]**7b** can also be used in competition experiments to evaluate non-radioactive inhibitors acting orthosterically at the acyltransferase

site. To exemplarily demonstrate this potential application, radio-TLC binding experiments of [^{18}F]**7b** to hTGase 2 were performed in the presence of increasing concentration of **7b** and two other acrylamide-based inhibitors (**A** and **C**, structures shown in Figure S6 in the Supporting Information). Again, the concentration of Ca^{2+} was adjusted to 0.2 mM and an incubation period of 5 min was chosen. The low Ca^{2+} concentration ensures that the reactions proceed slow enough to handle manually several reaction vials with different inhibitor concentrations while the short incubation period prevents that the IC_{50} values reach half of the employed enzyme concentration. The respective curves for the three inhibitors are shown in Figure 4D. Obviously, the IC_{50} values are higher than those obtained by the fluorescence polarisation assay[36] but the trend of the IC_{50} values within these three inhibitors is in accordance to the expectations. Compound **7b** exhibits the lowest IC_{50} followed by **A** and **C**. Interestingly, **7b** turned out to be more potent than **A** at pH 7.4 which is in accordance to their IC_{50} values at pH 8.0 (0.11 vs. 0.31 µM) measured by an in-house fluorescence polarisation assay.[36] However, this result is in contrast to the k_{inact}/K_I values of these two compounds at pH 6.5 (3,880 vs. 4,880 $M^{-1}s^{-1}$).[36] In this context, Miyahisa et al. recently published a procedure to derive k_{inact}/K_I values for unlabelled irreversible inhibitors using a radiolabelled probe in a radiometric endpoint competition assay.[53] By knowledge of the concentration of the radiotracer (probe, 0.011 µM) and its k_{inact}/K_I value (7,900 $M^{-1}s^{-1}$, this study), the IC_{50} value of the non-labelled inhibitor can be calculated using the following equation.

$$\left(\frac{k_{inact}}{K_I}\right)_{inhibitor} = \left(\frac{k_{inact}}{K_I}\right)_{probe} * \frac{[probe]}{IC_{50}} \qquad \text{(I)}$$

For compounds **7b**, **A** and **C** k_{inact}/K_I values of 45, 29 and 11 $M^{-1}s^{-1}$ were obtained, respectively. The reason for the low inactivation constants is the low Ca^{2+} concentration employed in these experiments (0.2 mM). However, as the relative inhibitory potencies should not vary at different Ca^{2+} concentrations and, thus, at different activity states of the enzyme, the ratio of these values can be used to calculate the inactivation constants of **A** and **C** at saturating Ca^{2+}

concentrations (3 mM). Consequently, k_{inact}/K_I values of 5,100 and 1,900 $M^{-1}s^{-1}$ can be derived for **A** and **C** at pH 7.4, respectively, which are in good accordance to the values determined at pH 6.5 using the fluorimetric assay method (4,880 and 1,620 $M^{-1}s^{-1}$). Therefore, this proves that compound **7b** (identical to compound **7b** in ref.[36] exhibits an increased inhibitory potency at pH 7.4 and 8.0 compared to pH 6.5, as indicated by the results of the direct binding experiments with [^{18}F]**7b**. Such a behaviour was not observed for the inhibition of TGase 2 by other N^{ε}-acryloyllysine piperazides (see Figure 9 right in Ref.[36]). Generally, the velocity of covalent bond formation should be largely not affected by the different pH values of 6.5 and 8.0 as the thiol group of the active site Cys residue might exhibit a pK_a value significantly lower than 6.5 due to the special microenvironment. In this context, for the cysteine protease papain, which is related to the transamidase domain of TGase 2 regarding protein fold and catalytic mechanism, an apparent pK_a value of 3.3 has been reported for the thiol group of Cys.[66] Therefore, the enhanced inhibitory potency of **7b** at pH values ≥7.4 might rather result from more favourable non-covalent interactions.

In summary, radio-TLC binding experiments with [^{18}F]**7b** offer a novel and convenient way to detect and characterise active site-directed agents or allosteric modulators of TGase 2's transamidase activity.

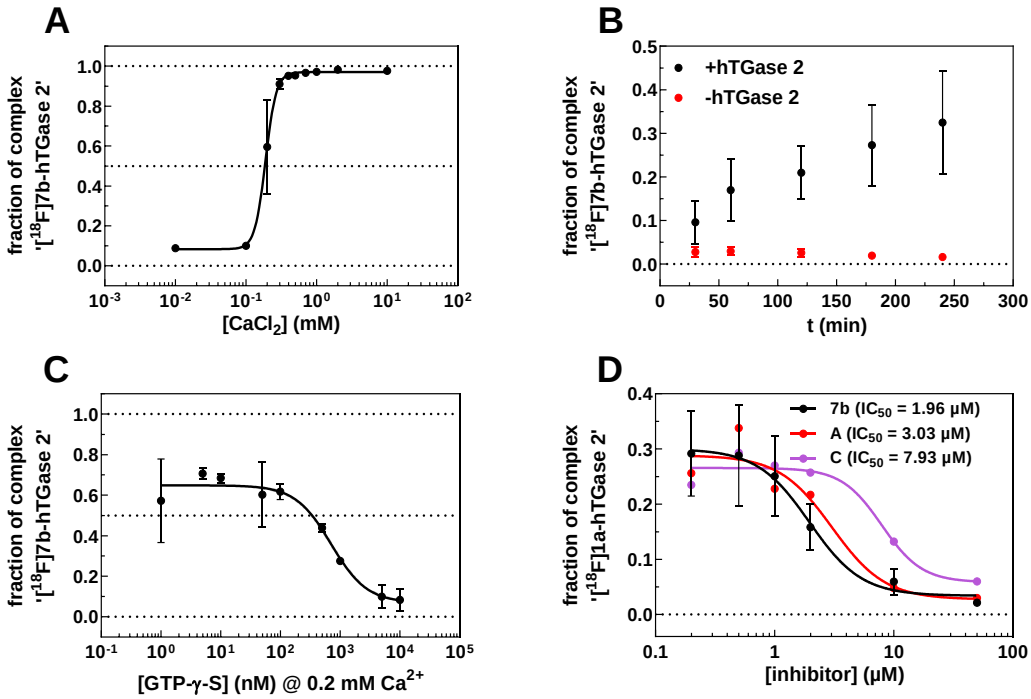

Figure 4. Radio-TLC experiments for binding of [^{18}F]7b to hTGase 2

A) Plot of (fraction of complex '[^{18}F]**7b**-hTGase 2')=f([$CaCl_2$]) including non-linear regression according to equation II. An EC_{50} value of 0.19 (±0.01) mM and a Hill coefficient of 5.7 (±1.8) were determined. **B)** Plot of (fraction of complex '[^{18}F]**7b**-hTGase 2')=f(t) at a $CaCl_2$ concentration of 0.1 mM. **C)** Plot of (fraction of complex '[^{18}F]**7b**-hTGase 2')=f([GTP-γ-S]) at a $CaCl_2$ concentration of 0.2 mM including non-linear regression according to equation II. An IC_{50} value of 710 (±240) nM and a Hill coefficient of 1.4 (±0.8) were determined. **D)** Plot of (fraction of complex '[^{18}F]**7b**-hTGase 2')=f([inhbitor]) at a $CaCl_2$ concentration of 0.2 mM including non-linear regressions according to equation II. Conditions: 30 °C, pH 7.4, 1 mM TCEP, 0.1 mg/mL (1.3 µM) hTGase 2. [^{18}F]**7b** and hTGase 2 were incubated for 5 min (**D**) or 30 min (**A** and **C**) at the distinct $CaCl_2$ and GTP-γ-S concentrations. Data shown are mean values (±SD) of 1-2 (**A**, **C** and **D**) or 5 (**B**) separate experiments. Fraction of complex '[^{18}F]**7b**-hTGase 2' refers to the ratio of the hTGase 2 associated ^{18}F-activity in relation to the total amount of ^{18}F-activity as determined densitometrically in the radio-TLC lane.

Radio-SDS-PAGE[67] experiments with cell lysates

As the results of the radio-TLC experiments clearly prove [^{18}F]**7b** to be a very sensitive probe for TGase 2, its suitability to detect the enzyme at the cellular level was evaluated. Due to the irreversible covalent bond formation at the enzyme's active site, detection of the enzyme-

inhibitor complex by radio-SDS-PAGE should be appropriate for that purpose. To prove this assumption, [^{18}F]**7b** alone and the complex formed upon incubation with hTGase 2 were subjected to electrophoretic separation. As shown in Figure 5A, the free radiotracer [^{18}F]**7b** is moving with the electrophoretic front, probably because it is included in negatively-charged micelles formed of SDS molecules. Analysis of [^{18}F]**7b** incubated with hTGase 2 for 20 min revelaed that the majority of the ^{18}F-activity is retained at the position that is in accordance with the molar mass of 77.4 kDa for the TGase 2 protein molecule. Incubation of [^{18}F]**7b** with hTGase 6, which has a comparable molar mass to hTGase 2 of 79.3 kDa, under identical conditions resulted in a radioelectrophoretic trace that displayed the bulk of activity at the front, whereas at the position of the enzyme only a very weak signal appeared. This result is in agreement to that of the radio-TLC experiment (Figure 3) demonstrating again hTGase 2-selective radiotracer binding. Hence, one can expect that a band appearing at the position corresponding to the molar mass of about 78 kDa will represent mainly hTGase 2 (this holds true at least for incubation periods of up to 30 min). For hTGase 2, distinct bands of ^{18}F activity were also visible at a molar mass greater than 80 kDa. These bands might indicate covalent multimers of hTGase 2 which arise from transamidative self-multimerisation as recently discovered.[68, 69]

On that basis, several cell lines were investigated for the presence of activatable[70] hTGase 2 in their cell lysates after incubation with [^{18}F]**7b**. In accordance with the data from Western blot expression analysis, which show distinct expression levels of hTGase 2 in A375 melanoma, MDA-MB-231 breast cancer, NCI-H292 lung cancer and HAEC endothelial cell lines, significant binding of [^{18}F]**7b** was detectable in these cell lines (Figure 5). In contrast, the expression level of the target enzyme and thus radiotracer binding was almost negligible in MeWo melanoma cell lysates (Figure 5A+B). Binding of [^{18}F]**7b** to hTGase 2 was furthermore detectable in the A375hS100A4 cells overexpressing the pro-metastatic S100A4 protein resulting from transfection with the corresponding gene. Interestingly, this cell line shows an even higher expression of hTGase 2 than the wild-type A375 cells and was therefore selected

for further investigations. Moreover, there seems to be a link between TGase 2-catalysed modification of S100A4 and its pro-metastatic action.[71-73] The selectivity of radiotracer binding to hTGase 2 in the A375hS100A4 cell lysates was proven by preincubation with the hTGase 2 inhibitors Z006, **7b** and **7a**. Compound Z006 is a commercially available peptidic diazoketone-based inhibitor which is selective for hTGase 2 over the hTGases 1, 3, 6 and hFXIIIa.[65] Compound **7a** exhibits potent inhibition of TGase 2 that is also highly selective over the hTGases 1, 3, 6 and hFXIIIa.[36] No protein band was detectable by radio-SDS-PAGE upon preincubation at 10 µM for 5 min with either of these compounds, which clearly demonstrates the specificity and selectivity of [^{18}F]**7b** (Figure 5A).

For the radio-SDS-PAGE experiments of the cell lysates, a sufficiently high concentration of [^{18}F]**7b** was chosen along with an appropriate period of incubation (25 min) to ensure labelling of all activatable hTGase 2 molecules. This was confirmed by unbound [^{18}F]**7b** detectable at the electrophoretic front (Figure 5A). Consequently, densitometric analysis of each lane of the radioluminographic images allows for determining the fraction of the complex [^{18}F]**7b**-hTGase 2 and enables a comparison of the different cell lines regarding their relative amount of activatable hTGase 2. The results are shown in Figure 5B together with the corresponding expression results of hTGase 2 obtained by Western blot. Both A375 cell lines exhibit the highest protein amount while the fraction of activatable hTGase 2 is comparable to or even lower than for MDA-MB-231, NCI-H292 and HAEC. Moreover, the highest amount of activatable hTGase 2 was determined in HAEC whose expression of that protein is significantly lower compared to the other cell lines except MeWo. This discrepancy between both data sets indicates that depending on the cell line not all hTGase 2 molecules present in the cell lysate are activatable or activation is somehow limited, which particularly seems to apply for cancer cell lines. Similar data were obtained by screening cell lysates using a fluorescence polarisation assay[36, 48] recently developed by us (unpublished results).

In a further radio-SDS-PAGE experiment the amount of the complex '[^{18}F]**7b**-hTGase 2' was exemplarily quantified for A375. For that purpose, a calibration curve was prepared by spotting defined activities of [^{18}F]**7b** on a TLC stripe, which was then placed under the same imaging plate as the gel of the radio-SDS-PAGE (see Figure S7 in Supporting Information). Knowledge of the molar activity, the activity concentration of [^{18}F]**7b**, the protein concentration and the 1:1 stoichemitry of radiotracer-TGase 2 interaction allow for the quantification of the bands around 78 kDa by means of the amount of activatable hTGase 2 per mass of cell lysate protein (Figure 5D). A concentration of 0.28 fmol/µg total protein was derived for A375. This concentration can be transformed into the number of hTGase 2 molecules per cell by using a correlation factor between cells and protein amount (for the correlation of protein amount *versus* A375 cells as well as the method to calculate hTGase 2 molecules per cell see Figure S8 in Supporting Information). According to this, around 12,000 hTGase 2 molecules per cell were labelled by [^{18}F]**7b**.

Radio-SDS-PAGE experiments with living cells

Encouraged by these results, the radiotracer's capability of detecting active hTGase 2 in viable cells, exemplarily in A375hS100A4 cells, was evaluated. As compound **7b** displayed a permeability coefficient >100 nm/s in the PAMPA assay,[36] the radiotracer [^{18}F]**7b** can be judged membrane-permeable and should be able to target transamidase-active intracellular TGase 2. Incubation of viable A375hS100A4 cells with [^{18}F]**7b** for 30 min resulted in no detectable band at the molecular mass corresponding to hTGase 2 (Figure 5C). This is not surprising as TGase 2 is largely transamidase-inactive under physiological conditions because it adopts predominantly the closed conformation due to a low cytosolic calcium concentration and high levels of purine nucleotides. However, the intracellular calcium levels can be increased by application of suitable ionophores such as ionomycin, which in turn stimulates the intracellular TGase 2 activity.[74-76] Indeed, incubating A375hS100A4 cells with [^{18}F]**7b** in the presence of ionomycin resulted in a radioelectrophoretic band at the molecular mass

corresponding to hTGase 2 (Figure 5C). In contrast, virtually no band was visible for the TGase 2-negative MeWo cells both in the absence and presence of ionomycin. These results unequivocally prove the capability of [^{18}F]**7b** to detect transamidase-active hTGase 2 in viable cells. Binding of [^{18}F]**7b** in A375hS100A4 cells was also investigated for incubations of up to 4 h without ionomycin. However, no [^{18}F]**7b** binding to hTGase 2 was detectable (Figure S9 in Supporting Information) indicating that despite the high expression of hTGase 2 in these cells no reactive enzyme is present under physiological conditions. The application of other reagents different from ionomycin, that were reported to elicit transamidase-active TGase 2 in other cell lines via various mechanisms,[77-80] did not result in the formation of the [^{18}F]**7b**-hTGase 2 complex in viable A375hS100A4 cells (see Figure S9 in Supporting Information), which indicates that the corresponding pathways for TGase 2 activation do not seem to be active in this cell line.

As done for A375 cell lysate, the amount of the complex '[^{18}F]**7b**-hTGase 2' detectable after incubation with [^{18}F]**7b** in the presence of ionomycin was quantified for vital A375 cells (Figure 5D). A concentration of 0.009 fmol/µg total protein was derived, which is 31-times lower than the concentration in cell lysates. This corresponds to approximately 400 hTGase 2 molecules per cell and indicates the high sensitivity of that radiotracer approach to detect active hTGase 2 in cells.

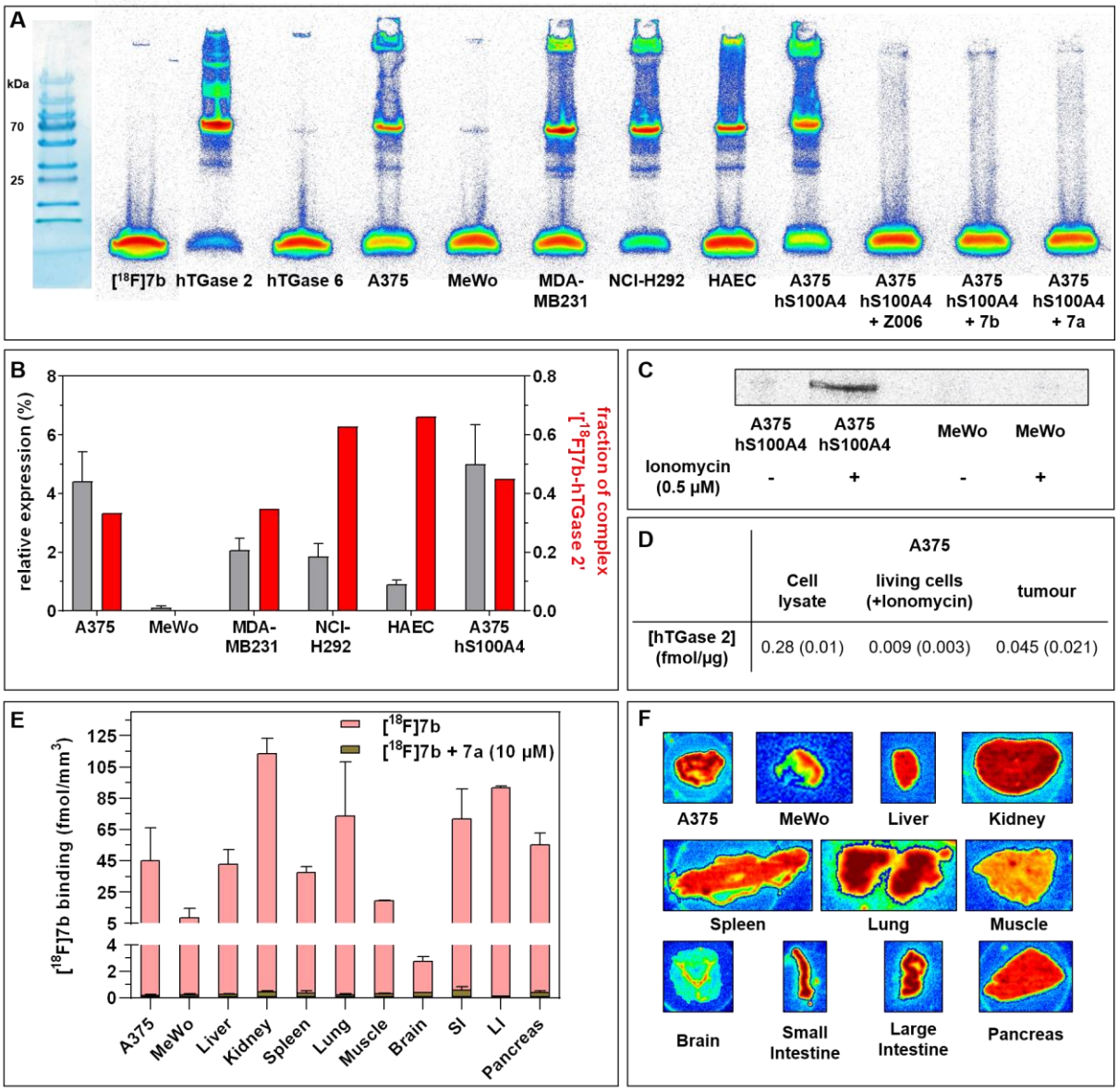
A
kDa
70
25
[18F]7b
hTGase 2
hTGase 6
A375
MeWo
MDA-MB231
NCI-H292
HAEC
A375 hS100A4
A375 hS100A4 + Z006
A375 hS100A4 + 7b
A375 hS100A4 + 7a
B
relative expression (%)
fraction of complex 'r[18F]7b-hTGase 2'
A375
MeWo
MDA-MB231
NCI-H292
HAEC
A375 hS100A4
C
A375 hS100A4
A375 hS100A4
MeWo
MeWo
Ionomycin (0.5 µM)
-
+
-
+
D
A375
Cell lysate
living cells (+Ionomycin)
tumour
[hTGase 2] (fmol/µg)
0.28 (0.01)
0.009 (0.003)
0.045 (0.021)
E
[18F]7b binding (fmol/mm3)
[18F]7b
[18F]7b + 7a (10 µM)
A375
MeWo
Liver
Kidney
Spleen
Lung
Muscle
Brain
SI
LI
Pancreas
F
A375
MeWo
Liver
Kidney
Spleen
Lung
Muscle
Brain
Small Intestine
Large Intestine
Pancreas

Figure 5. Radio-SDS-PAGE experiments and autoradiography of tissue sections with [^{18}F]7b

A) Radioluminogram of radio-SDS-PAGE electropherogram for [^{18}F]**7b** binding on isolated enzymes and cell lysates. Conditions: pH 8.0, 30 °C, 3 mM $CaCl_2$, 1 mM TCEP for recombinant TGases and 1 mM DTT for cell lysates; 20 min incubation period with [^{18}F]**7b**; total protein amount per lane: 100 ng of hTGase 2, 50 ng of hTGase 6, 50 µg of cell lysates from A375, MeWo, MDA-MB231, NCI-H292 and A375-hS100A4 and 15.7 µg of HAEC cell lysate; 10 µM of the respective inhibitor (5 min preincubation period before addition of [^{18}F]**7b**). Bands are shown in rainbow colours. On the left side, the Coomassie stained protein ladder from 10 to 250 kDa is shown. **B**) Densitometric Western blot analysis (grey columns, mean values ± SEM, n≥3) and densitometric analysis (fraction of complex '[^{18}F]**7b**-hTGase 2', red columns) of the radioluminogram in **A** for the different cell lysates. For HAEC, fraction of complex '[^{18}F]**7b**-hTGase 2' was multiplied by factor 3.2 (50/15.7 µg) to obtain comparable data to the other cell lines. **C**) Section of radioluminogram around 78 kDa of radio-SDS-PAGE electropherograms for [^{18}F]**7b** binding in living cells upon stimulation of intracellular TGase 2 activity with the calcium ionophor ionomycin. Incubation of living cells in DMEM containing [^{18}F]**7b** for 30 min at 37°C prior to cell lysis. Bands are shown in greyscale. **D**) Summary of hTGase 2 concentration (fmol/µg total protein) obtained in the different A375 models. For conversion of A375 tumour data in **E** (fmol/mm^3), a tissue densitiy of 1.03 g/cm^3 was assumed. **E**) Overview of hTGase 2 concentration (fmol/mm^3, mean values ± SD, n≥3) obtained by analysis of radioluminograms from in vitro autoradiography of tissue slices (organs and tumours from healthy and A375 / MeWo xenograft bearing NMRI nude mice (nu/nu), respectively). Binding of [^{18}F]**7b** was almost completely blocked in the presence of **7a**. **F**) Sections of radioluminograms for the distinct tumour and organ slices. Colouring are shown in rainbow colours.

Autoradiography of tissue sections

For the ^{11}C- and ^{18}F--labelled TGase 2 inhibitors described by van der Wildt et al., the authors demonstrated the capability of the tracers to detect hTGase 2 in a complex biological matrix by autoradiography of tumour sections.[43, 44] Inspired by this approach, we envisaged to perform similar experiments by incubation of sections of A375 (hTGase 2 positive) and MeWo (hTGase 2 negative) tumour xenografts and different organs of healthy mice with [^{18}F]**7b**. The resulting radioluminograms were analysed and the concentration of hTGase 2 was quantified in fmol per volume (mm^3). Initially, binding of [^{18}F]**7b** to sections of A375 and MeWo tumour xenografts were evaluated under different conditions for activation and selective blocking of hTGase 2 (Figure 6). For A375, only negligible binding of [^{18}F]**7b** was observed in PBS buffer

(pH 7.4) alone (0.2 fmol/mm^3), which significantly increased in the presence of $CaCl_2$ (3 mM; 30.9 fmol/mm^3) and even more with $CaCl_2$ and DTT (5 mM; 45.5 fmol/mm^3). These results are in accordance to the recently published ^{11}C -labelled acrylamide derivative and highlight a low non-specific binding of [^{18}F]**7b** and the well-known dependence of the transamidase activity on Ca^{2+} and a reducing milieu. However, it should be pointed out that the artificial conditions (3 mM $CaCl_2$ / 5 mM DTT) cause all activatable TGase 2 molecules to be activated and any conclusion for regarding the in situ activity of that enzyme cannot be derived. In the presence of Ca^{2+}/DTT and the non-radioactive compound **7b** or **7a** (10 µM each) binding of [^{18}F]**7b** is reduced to the level without Ca^{2+}/DTT (0.3 fmol/mm^3 and 0.2 fmol/mm^3, respectively), which confirms selective and specific binding of [^{18}F]**7b** to hTGase 2. For MeWo, binding of [^{18}F]**7b** also increased in the presence of Ca^{2+}/DTT (0.1 *versus* 9.0 fmol/mm^3), however, binding is 5-times lower than for A375. This result is in apparent contrast to data from Western blot and radio-SDS-PAGE which indicated absence of hTGase 2 in MeWo cells (Figure 5B). However, Western blot of lysates from MeWo tumour xenografts confirmed the presence of TGase 2. Worth of note, densitometric Western blot analysis revealed a similar ratio of the TGase 2 amount in A375 and MeWo tumours compared to the results from radiotracer binding (≈5, see Figure S10 in Supporting Information). Potentially, the transition from cell monolayer culture to a xenograft tumour model can alter the protein expression profile of cancer cells.[81] Furthermore, murine (m) TGase 2 from cells which infiltrate the xenograft tissue during tumour growth has to be considered as [^{18}F]**7b** is also reactive towards mTGase 2 (a k_{inact}/K_I value of 3,990 $M^{-1}s^{-1}$ for **7b** was determined recently).[36] The presence of mouse cells in A375 and MeWo tumour xenografts was confirmed by exemplary immunohistochemical stainings for macrophages (CD68) and endothelial cells (CD31) (Figure 7). Therefore, the reason for observed significant binding of [^{18}F]**7b** to MeWo tumour sections originates most likely from the reaction of the radiotracer with mTGase 2 originating from infiltrated mouse cells.[82, 83]

By assuming a density of 1.03 g/cm^3,[84] the obtained concentration for A375 (in fmol/mm^3) was transformed into fmol/µg tumour tissue to compare the value with concentrations in cell lysate

and living cells. Thus, a value of 0.045 fmol/µg tumour tissue has been derived, which is 6-times lower than the concentration in lysates of isolated A375 cells (Figure 5D). This tendency appears to be reasonable as the heterogenous composition of the tumour might reduce the amount of TGase 2 per tissue mass compared to a cell monolayer.

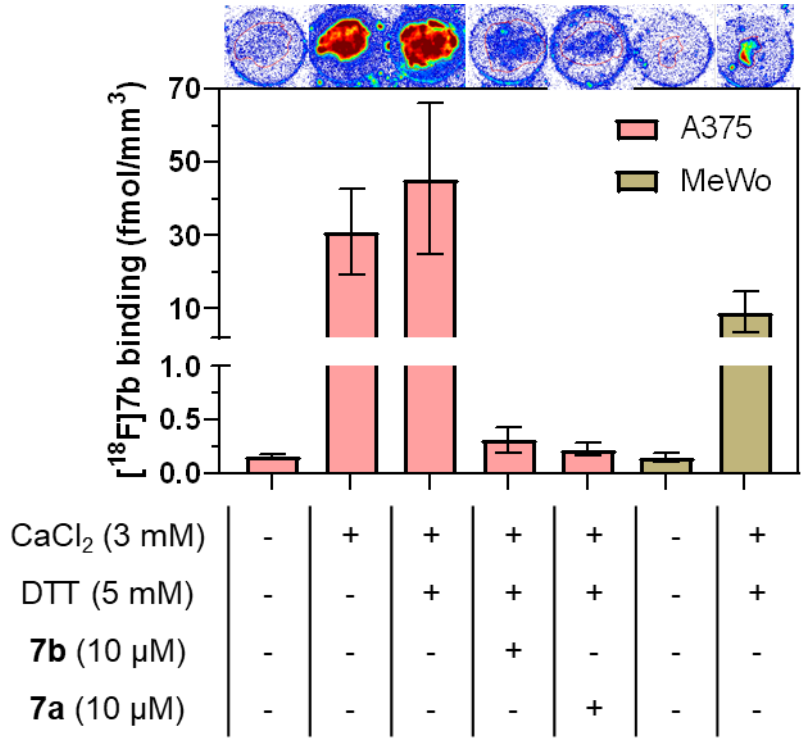

Figure 6. Testing [^{18}F]7b binding in tumour sections under different conditions

Binding results for [^{18}F]**7b** in tumour slices (fmol/mm^3, mean values ± SED, n≥3) obtained by analysis of radioluminograms from autoradiography. Exemplary sections of radioluminograms for the respective tumours are shown above the diagram (colouring in rainbow colours).

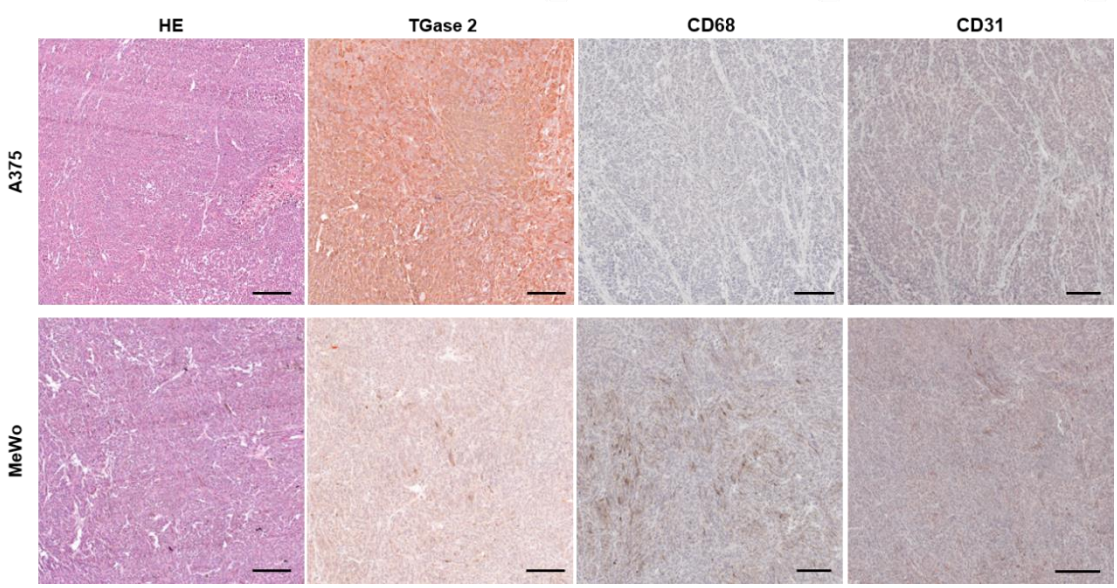

Figure 7. Immunohistochemical stainings of A375 and MeWo tumour slices

Exemplary images of Hematoxylin & Eosin staining (basophilic structures in blue, eosinophilic structures in red) as well as immunohistochemical staining of TGase 2 (in red-brown, cell nuclei in blue), CD68 (pan-macrophages in red-brown, cell nuclei in blue) and CD31 (endothelial cells in red-brown, cell nuclei in blue) are shown for A375 and MeWo tumour samples (scale bar: 200 µM). See Figure S11 in Supporting Information for respective isotype controls.

Due to the similar reactivity of [^{18}F]**7b** towards mTGase 2, it was envisaged to screen different mouse organs via autoradiography of tissue sections for their TGase 2 concentration. Tissue slices of different organs were incubated in the presence of $CaCl_2$/DTT for maximal activation of mTGase 2. Control incubations were done with compound **7a** as blocking agent. The obtained binding data and respective sections of the radioluminogram for the different organs are summarised in Figure 5E+F together with the data and sections for the A375 and MeWo tumours. As expected due to the known ubiquitous expression of TGase 2 in mammals, significant binding of [^{18}F]**7b** was observed in all studied organs with the highest value obtained in kidney (113.9 fmol/mm^3) followed by large intestine (92.2 fmol/mm^3), lung (74.3 fmol/mm^3), small intestine (72.2 fmol/mm^3) and pancreas (55.8 fmol/mm^3). Moreover, these concentrations were found to be higher than those for A375 tumour tissue (45.5 fmol/mm^3). This might reveal the same phenomenon as described before for [^{18}F]**7b** binding to cell lysates

which is higher for HAEC than for A375 even though the latter one exhibits the higher protein expression (Figure 5B). The lowest concentration by far was determined in tissue slices of the brain (2.8 fmol/mm^3). However, a distinct activity enrichment is visible in the horizontal brain section in the form of a C-shaped structures which could represent the lateral ventricle.[85] In this context, expression or function of TGase 2 in ependymal cells lining the ventricular system are not characterised so far.[86]

To the best of our knowledge, the quantitative screening for activatable TGase 2 in organs (by means of fmol/mm^3 or fmol/µg) represents the first study of its kind. The group of Hitomi used FITC-labelled, peptidic acyl donor substrates selective for TGase 1, TGase 2 and TGase 6, respectively, to detect the active enzymes *in vitro* in whole-body slices of mice. The conditions for activation were similar to the present ones (5 mM $CaCl_2$, 1 mM DTT, pH 8.0). Worth of note, a distinct staining for TGase 2 was seen in most parts of the mouse while for both TGase 1 and 6 the skin epidermis was predominantly stained.[87, 88] As a consequence of using an acyl donor substrate, detection of active TGase 2 might be limited by the availability of endogenous acyl acceptor substrates. Moreover, correlating the intensity of fluorescence-based images to concentration is sophisticated.[89] In contrast, irreversible inhibitors such as [^{18}F]**7b** label the enzyme directly in a 1:1 stoichiomitry and allow a reliable quantification of the signal via the radiolabel as demonstrated herein.

Overall, the results from the autoradiography of tissue sections indicate the high potential of radiotracer [^{18}F]**7b** to detect TGase 2 even in complex biological matrices. Furthermore, the data provide valuable information for further *in vivo* studies of [^{18}F]**7b** or other TGase 2 targeting molecules in healthy and tumour bearing mice.

Conclusion

Compound **7b** was recently described by our group as a potent and selective TGase 2 inhibitor.[36] The 2-fluoropyridine moiety renders **7b** suitable for the synthesis of its ^{18}F-analogue

to study the physiology of TGase 2 *in vitro* and *in vivo* with exceptional sensitivity. For the radiosynthesis of [^{18}F]**7b**, two precursor compounds were evaluated with the trimethylammoniopyridine derivative **8** being significantly more appropriate than the nitro pyridine derivative **7a** in terms of labelling yields and formation of side products. Using **8**, a reliable radiosynthesis has been established which provides [^{18}F]**7b** in high yields and excellent (radio)chemical purities.

The kinetics of the irreversible interaction of this radiotracer with hTGase 2 was assessed by radio-TLC experiments which allowed for the discrimination between free radiotracer and the radiotracer-protein complex. Hence, the inhibitory potencies of [^{18}F]**7b** were determined at different pH values, which were not accessible so far with conventional assay methods due to inherent limitations. Moreover, by careful adjustment of the assay conditions, [^{18}F]**7b** was used to determine binding of Ca^{2+}- and GTP-γ-S to hTGase 2. In this context, the titration with Ca^{2+} in the presence of [^{18}F]**7b** provided also the number of Ca^{2+} ions which can bind to hTGase 2. The obtained result (5 to 6 Ca^{2+} ions) is in excellent accordance to other methods published in the literature. Furthermore, the inhibitory potency of non-radioactive inhibitors can be quantified. The suitability of [^{18}F]**7b** to target TGase 2 was also demonstrated in living cells and cell lysates by radio-SDS-PAGE. The absence of further radioactive bands other than the one corresponding to the molecular mass of TGase 2 proved unambiguously the selectivity and specificity of the radiotracer towards TGase 2. Radiotracer [^{18}F]**7b** can pass the cell membrane and interact with TGase 2, however, no binding was detected in healthy cells, which confirms the widely accepted view that TGase 2 is not active in cells under physiological conditions. Furthermore, autoradiography experiments proved the binding of [^{18}F]**7b** to TGase 2 even in more complex biological objects, such as tissue slices. Using this approach, quantitative data on the expression of activatable TGase 2 in different mouse organs and tumour xenografts were collected for the first time.

By summing up the results for cell lysates, living cells and tissue sections it is obvious that a discrepancy exist between the relative expression of TGase 2 (proteome), the amount of activatable TGase 2 and the amount of active TGase 2 (activome[90]) with the general trend that the absolute amount significantly reduces in the same order. Moreover, there are differences between the cell lines with higher protein expression but lower activatable TGase 2 amount in non-tumour cells compared to tumour cells. The reasons for this phenomenon need to be further investigated. However, as shown in this study, a radiolabelled activity-based probe such as [^{18}F]**7b** can be highly suitable to sensitively measure the activity status of TGase 2 in different matrices. This supports the further understanding of the physiology of TGase 2 and will enable the radiotracer's use as activity-based probe for the sensitive detection of TGase 2 within biologically and pharmacologically motivated studies of this unique enzyme. Furthermore, this study illustrates how biological questions, that would be otherwise difficult to resolve, can be addressed through the synthesis of new radiotracers using carefully optimised radiochemical methodology.

The obtained information on expression and activity of TGase 2 activity will advance the evaluation of [^{18}F]**7b** as PET tracer for imaging studies *in vivo* and provide support towards selection of animal disease models with active TGase 2 for PET and SPECT imaging, also with regards to other radiolabelled inhibitors of this enzyme. Considering the fact that no active TGase 2 has been detected in healthy living cells, *in vivo* studies will also aim at answering the general question about the feasibility of active TGase 2 as a target for activity-based radiotracers. Current studies are focused on the radiopharmacological evaluation of [^{18}F]**7b** *in vivo* in healthy and tumour xenograft-bearing mice. In this context, the pharmacokinetic properties of this compound, particularly its metabolic stability, will be addressed in detail.

Experimental Section

General

The synthetic procedures and analytical data for compounds **3**, **7a**, **7b**, **A** and **D** along with all intermediate products were described previously.[36] Therefore, detailed experimental procedures and analytical data are given for precursor **8** and its intermediate products via the two different synthetic routes and for the side-products **9a** and **11** (Supporting Information). The purity of precursors **1a**, **2a**, **2b** and **8** as well as reference compounds **1b** and **7b** proved to be ≥95%, analyzed by a UPLC−diode-array detector−MS (UPLC− DAD−MS) system from Waters (ACQUITY UPLC I-Class System including a ACQUITY UPLC PDA eλ-Detector coupled to a Xevo TQ-S mass spectrometer).

Radiosynthesis

Processing of [^{18}F]fluoride for radiosynthesis under classic conditions

No-carrier-added aqueous [^{18}F]fluoride was produced in a IBA CYCLONE 18/9 cyclotron or in a ACSI TR-FLEX cyclotron by irradiation of [^{18}O]H_2O through the $^{18}O(p,n)^{18}F$ nuclear reaction. The aqueous [^{18}F]fluoride (1–3 GBq) was adsorbed on an anion-exchange cartridge (QMA Plus Short from Waters preconditioned with 10 mL water) and eluted with a solution (1 mL) of 10 mg (or 5 mg) Kryptofix 222 and 1.8 mg (or 0.9 mg) K_2CO_3 in 14% H_2O/CH_3CN into a conical glass vial equipped with a screw cap and rubber septum. Removal of H_2O was accomplished by azeotropic distillation with CH_3CN in a stream of nitrogen gas at 90 °C with stirring. In total, 4×2 mL of CH_3CN were added and the remaining residue was dissolved in the corresponding reaction medium.

Processing of [^{18}F]fluoride for radiosynthesis under "minimalist" conditions

This procedure was accomplished according to the protocol of Richarz et al.[46] The aqueous [^{18}F]fluoride (1–11 GBq) was adsorbed on an anion-exchange cartridge (QMA Plus Light carbonate from Waters preconditioned with 10 mL water) followed by flushing of the cartridge with methanol (2×2 mL). The [^{18}F]fluoride was eluted with a solution (500 µL) of the respective trimethylammonium precursor (e.g. 3 mg) in methanol followed by flushing of the cartridge with methanol (500 µL) into a conical glass vial equipped with a screw cap and rubber septum. Removal of methanol was accomplished in a stream of nitrogen gas at 70 °C with stirring. The remaining residue was dissolved in the corresponding reaction medium.

*Preparation of [^{18}F]**7b** by the optimised procedure using precursor **8** under "minimalist" conditions*

CH_3CN (500 µL) was added to the [^{18}F]fluoride- and trimethylammonium precursor-containing residue obtained after removal of methanol and brought to the reaction temperature of 110 °C for 10 min. The reaction solution was cooled on ice for a short time (2 min) and water (50 µL) was added. An aliquot of the reaction mixture (10 µL) was withdrawn for analysis of the crude mixture by radio-TLC and analytical radio-HPLC. The remaining reaction mixture was filtered (PTFE filter, pore size of 0.22 µm) and the filtrate was purified by semi-preparative radio-HPLC. The peak representing the product was collected (approximately 5 mL) and immediately diluted with H_2O to a overall volume of 50 mL. The resulting solution was subjected to solid-phase extraction by using a 500 mg LiChrolut RP-18 (40-63 µm) or Chromafix C-18 ec (s) cartridge (preconditioned with 2 mL ethanol and 10 mL water). The cartridge was washed with water (2×2 mL) and the product was eluted with ethanol (2×0.5 mL). An aliquot (10 µL) of that solution was withdrawn for quality control (determination of molar activity as well as (radio)chemical purity by analytical radio-HPLC and radio-TLC). The product solution was

evaporated to a volume of <100 µL, cooled on ice for a short time (2 min) and a defined volume was withdrawn for further experiments.

Enzymatic Radio-TLC experiments

All measurements were conducted at 30 °C in 0.5 mL Eppendorf tubes. The following buffer systems were used: assay buffer pH 6.5/7.4/8.0 (100 mM MES for pH 6.5 or MOPS pH 7.4 and 8.0, varying $CaCl_2$ concentrations, 50 µM EDTA, adjusted to the respective pH values with 1 M NaOH) and enzyme buffer (100 mM MES, 0 or 3 mM $CaCl_2$, 10 mM TCEP, 20% (v/v) glycerol, adjusted to pH 6.5 with 1 M NaOH). The buffers were stored at 0 °C for periods of up to two weeks and freshly prepared after that period. For the radio-TLC experiments, a considerable lower molar activity of 1 GBq/µmol for [^{18}F]**7b** was assumed during planning of experiment to ensure that [enzyme] >> [[^{18}F]**7b**] (the determined molar activities for these experiments were between 5 and 18 GBq/µmol resulting in a 5 to 18 times higher [enzyme] compared to [[^{18}F]**7b**]). For analysis of the reactions, an aliquot (5-10 µL) was withdrawn at the distinct time point and added to the same volume of 1 M HCl (stop of the reaction); 2 µL of that solution were finally spotted on a TLC plate. Further processing was conducted as described in the section Chromatography.

*Radiometric determination of the inactivation constants k_{inact}/K_I of [^{18}F]**7b** towards hTGases at different pH values*

A 100 µM solution of [^{18}F]**7b** in assay buffer (3 mM $CaCl_2$) was prepared. This stock solution (5 µL) was added to the respective assay buffer (445 µL, 3 mM $CaCl_2$). The reactions were initiated upon addition of the respective hTGase stock solution (50 µL, 1 mg/mL for hTGase 2 and 0.5 mg/mL for hTGase 6 which corresponds to 10 and 5 µM active enzyme concentration, respectively). The time points for withdrawal of aliquots for analysis were 0, 5, 10, 15, 20, 25 and 30 min. To ensure that [^{18}F]**7b** is stable under these conditions, a similar reaction mixture without the presence of enzyme was analysed after 30 min. Within the obtained

radioluminograms, the spots of [^{18}F]**7b** and [^{18}F]**7b**-hTGase were integrated. The fraction of 'free [^{18}F]**7b**' was plotted against the time (in s) and the resulting curve was analysed by nonlinear regression according to the equation of one-phase decay in Prism. The obtained k_{obs} value (in s^{-1}) represents (k_{inact}/K_I)*[enzyme] as [enzyme] >> [^{18}F]**7b**. Division by [enzyme] provided the inactivation constant k_{inact}/K_I (see Figure S5 in Supporting Information).

*Determination of the Ca^{2+}-dependence of [^{18}F]**7b** binding to hTGase 2 at pH 7.4*

A 10 µM solution of [^{18}F]**7b** in assay buffer (pH 7.4, $CaCl_2$-free) was prepared. This stock solution (6 µL) was added to assay buffer (48 µL, pH 7.4) containing distinct concentrations of $CaCl_2$ (0.0125, 0.125, 0.25, 0.375, 0.5, 0.625, 0.875, 1.25, 2.5 and 12.5 mM). The reactions were initiated upon addition of the hTGase 2 stock solution in enzyme buffer (6 µL, 1 mg/mL, $CaCl_2$-free). After 30 min, an aliquot of each solution was withdrawn. The proportion of complex '[^{18}F]**7b**-hTGase 2' was plotted against [$CaCl_2$] (in mM) and the resulting curve was analysed by nonlinear regression according to equation II to obtain the EC_{50} value for Ca^{2+} and the Hill coefficient n_H.

$$\frac{[^{18}\mathbf{F}]\mathbf{1a}\text{–hTGase 2}}{[^{18}\mathbf{F}]\mathbf{1a}} = \text{Bottom} + \frac{(\text{Top} - \text{Bottom}) \times [\text{CaCl}_2]^{\text{nH}}}{[\text{CaCl}_2]^{\text{nH}} + \text{EC}_{50}{}^{\text{nH}}} \qquad \text{(II)}$$

*Influence of GTP-γ-S on [^{18}F]**7b** binding to hTGase 2 at pH 7.4*

A 10 µM solution of [^{18}F]**7b** in assay buffer (pH 7.4, 2 mM $CaCl_2$) was prepared. This stock solution (6 µL) was added to assay buffer (48 µL, $CaCl_2$-free) containing distinct concentrations of GTP-γ-S (0, 1.25, 6.25, 12.5, 62.5, 125, 625, 1,250, 6,250 and 12,500 nM). The reactions were initiated upon addition of the hTGase 2 stock solution in enzyme buffer (6 µL, 1 mg/mL, $CaCl_2$-free). After 30 min, an aliquot of each solution was withdrawn. The fraction of complex '[^{18}F]**7b**-hTGase 2' was plotted against [GTP-γ-S] (in nM) and the resulting curve was analysed by nonlinear regression according to equation II to obtain the IC_{50} value for GTP-γ-S and the Hill coefficient n_H.

*Using [^{18}F]**7b** binding to hTGase 2 for competitive inhibition experiments*

A 10 µM solution of [^{18}F]**7b** in assay buffer (pH 7.4, 2 mM $CaCl_2$) was prepared. This stock solution (3 µL) was added to 12.5% DMSO/assay buffer (3 µL, pH 7.4, $CaCl_2$-free) containing distinct concentrations of compounds **7b**, **C** or **D** (0, 2, 5, 10, 20, 100 and 500 µM). To these mixtures, assay buffer (21 µL, pH 7.4, $CaCl_2$-free) was added. The reactions were initiated upon addition of the hTGase 2 stock solution in enzyme buffer (3 µL, 1 mg/mL, $CaCl_2$-free). After 5 min, an aliquot of each solution was withdrawn. The fraction of complex '[^{18}F]**7b**-hTGase 2' was plotted against [inhibitor] (in µM) and the resulting curve was analysed by nonlinear regression according to equation II to obtain the IC_{50} value for the respective inhibitor and the Hill coefficient n_H.

*Determination of [^{18}F]**7b** binding to hTGase 2 at a low Ca^{2+} concentration (100 µM)*

A 10 µM solution of [^{18}F]**7b** in assay buffer (pH 7.4, 1 mM $CaCl_2$) was prepared. This stock solution (6 µL) was added to assay buffer (48 µL, pH 7.4, $CaCl_2$-free). The reaction was initiated upon addition of the hTGase 2 stock solution in enzyme buffer (6 µL, 1 mg/mL, $CaCl_2$-free). After distinct time points (0.5, 1, 2, 3 and 4 h) an aliquot (2 µL) of the solution was withdrawn. The fraction of complex [^{18}F]**7b**-hTGase 2 was plotted against the time. To ensure that [^{18}F]**7b** is stable under these conditions, a similar reaction mixture without the presence of enzyme was analysed after 4 h.

Radio-SDS-PAGE experiments

Radio-SDS-PAGE was performed as horizontal PAGE using the Multiphor II electrophoresis system from GE Healthcare. Both the gel and the buffer strips were obtained from GE Healthcare (ExcelGel SDS, gradient 8-18). The following buffer systems were used: assay buffer pH 7.4/8.0 (100 mM MOPS, varying $CaCl_2$ concentrations, 50 µM EDTA, adjusted to the respective pH value with 1 M NaOH), lysis buffer (modified RIPA buffer; 150 mM NaCl, 50 mM

Tris pH 8.0, 1 µg/mL Leupeptin, 1 mM PMSF, 5 mM NaF, 1 mM $NaVO_4$, 1 mM DTT), SDS-PAGE sample buffer: 312.5 mM Tris-HCl pH 6.8, 10% (w/v) SDS, 40% (w/v) glycerol, 5% (w/v) ß-mercaptoethanol, bromophenol blue. Radioactive bands were visualised by using the Fujix Bas2000 TR radioluminography system or the Amersham Typhoon 5 Biomolecular Imager. The radioluminograms were analysed by the software AIDA (Advanced Image Data Analyzer, version 5.1 SP4 Build 1244). For quantification of the radioactive bands, a TLC stripe with spots of defined activity of [^{18}F]**7b** was placed under the same imaging plate as the gel. For the radio-SDS-PAGE experiments, the molar activity of [^{18}F]**7b** was assumed to be 5 GBq/µmol during planning of experiment as the determination of molar activity was delayed compared to start of the biological experiments. The determined molar activities for these experiments were up to 100 GBq/µmol. However, concentration of [^{18}F]**7b** was still higher than enzyme concentration in cell lysates or cells which ensures labelling of all activatable TGase 2 molecules.

*Binding of [^{18}F]**7b** to recombinant hTGases*

A 100 µM solution of [^{18}F]**7b** in assay buffer (pH 8.0, 4 mM $CaCl_2$) was prepared. This stock solution (5 µL) was added to assay buffer (445 µL, pH 8.0, 3 mM $CaCl_2$). The reaction was initiated upon addition of the respective hTGase stock solution (50 µL, 1 mg/mL for hTGase 2 and 0.5 mg/mL for hTGase 6) and the mixture was incubated for 20 min at 30 °C. To show the movement of [^{18}F]**7b** during the gel electrophoresis, a similar reaction mixture without the presence of enzyme was prepared. An aliquot of this solution was withdrawn (2.5 µL) and diluted with assay buffer II (37.5 µL) before SDS-PAGE sample buffer (10µL) was added. This sample was heated to 99 °C for 5 min and an aliquot (20 µL) of the mixture was applied to the gel.

*Binding of [^{18}F]**7b** to hTGase 2 in cell lysates*

The human metastatic melanoma cell lines A375 and MeWo were obtained from the ATCC. Furthermore, the tumour cell lines NCI-H292 (Bayer HealthCare), MDA-MB231 (LGC standard), the transgenic melanoma cell line A375-hS100A4[91] and human aortic endothelial cells (HAEC, PELOBiotec) were used for the experiments. A375 and MeWo were cultured in Dulbecco's modified Eagle's medium (DMEM) supplemented with 10% (v/v) fetal calf serum (FCS) and penicillin/streptomycin (P/S, 1 U/mL, all reagents from Biochrom) at 37°C in a humidified atmosphere with 5% CO_2. MDA-MB231 were cultured in Leibovitz L-15 medium (Sigma-Aldrich) without CO_2 and NCI-H292 were cultured in RPMI 1640 medium (Biochrom), both media contained the same supplements as mentioned above. HAEC were cultured in Endothelial Cell Growth Medium enhanced (PELOBiotech). A375-hS100A4 were cultivated in a similiar medium as A375 but supplemented with G418 (1.2 mg/mL, Biochrom) instead of P/S. All cells were monthly tested to be mycoplasma-negative with Venor® GeM Mycoplasma Detection Kit (Minerva Biolabs). Cell pellet was collected by detaching cells, grown in a 75 cm² culture flask (Greiner Bio-One), with trypsin/EDTA solution (0.05%/0.02%) in PBS. Afterwards, the cell suspension was centrifuged (3 min, 300×g) and the pellet was washed twice with PBS. For cell lysis, the pellet was resuspended in lysis buffer (50 µL), incubated on ice for 30 min and applied to ultrasound. Subsequently, the cell lysate was spinned for 15 min at 4°C at 15,000×g and the supernatant was transferred into a fresh tube. The protein content was determined with a BCA protein assay (ThermoFisher) according to the manufacturer's protocol. The lysate was stored at -60 °C.

A 1 µM solution of [^{18}F]**7b** in assay buffer (4 mM $CaCl_2$) was prepared. The cell lysate was diluted with assay buffer (4 mM $CaCl_2$) to a protein concentration of 3.33 g/L (1.10 g/l for HAEC). To this solution (37.5 µL), the 1 µM solution of [^{18}F]**7b** (2.5 µL) was added and the mixture was incubated for 25 min at 30 °C. For blocking experiments, the diluted cell lysates were preincubated with TGase 2-inhibitors (10µM, **Z006** (Zedira), **7b** and **7a**, respectively) for

5 min before [^{18}F]**7b** was added (stock solutions 4 mM of the inhibitors were prepared in DMSO). Afterwards, the reaction mixture was mixed with SDS-PAGE sample buffer (10 µL). This sample was heated to 99 °C for 5 min and an aliquot (20 µL) of the mixture was applied to the gel.

*Binding of [^{18}F]**7b** to hTGase 2 in living cells*

5-8*10^5 of A375, A375-hS100A4 or MeWo cells were seeded into a 6-well plate (Greiner) and grown for 24 h. A375-hS100A4 cells were further grown for 24 h in DMEM containing carbonylcyanide 3-chlorophenylhydrazone (CCCP, Acros Organics, 10 µM, stock 2 mM in DMSO), in EBSS (Earles's Balanced salt solution) alone or with MG132 (Sigma-Aldrich, 5 µM, stock 1 mM in DMSO) and in DMEM (pH 6.15, adjusted with 1 M HCl). Afterwards, cells were washed with PBS, then cultivated with DMEM (1 mL, 0-0.1% FCS) containing [^{18}F]**7b** (1 µM) or with DMEM containing [^{18}F]**7b** (1 µM) and the calcium ionophore ionomycin (0.5 µM, Sigma-Aldrich) for up to 4 h at 37 °C. Afterwards, cells were washed twice with PBS and lysed with lysis buffer (100 µL per well). The lysed cells were transferred into a tube using a cell scraper and a pipette and applied to ultrasound. Samples were centrifuged for 15 min at 15,000×g at 4 °C. Subsequently, the supernatant (20 µL) was mixed with SDS-PAGE sample buffer (5 µL). This sample was heated to 99 °C for 5 min and an aliquot (20 µL) of the mixture was applied to the gel.

Binding of [^{18}F]7b to tissue and tumour sections

Animal experiments were carried out according to the guidelines of the German Regulations for Animal Welfare. The protocol was approved by the local Ethical Committee for Animal Experiments (reference numbers DD24-9168.11-4/2012-1 and DD24.1-5131/449/49). The protocol for generation of melanoma xenograft models and preparation of organs and tumours followed the protocols published in detail elsewhere.[92, 93]

Organs and tumours (A375 / MeWo) were extracted from healthy and tumour xenograft bearing NMRI nude mice, respectively and were deep-frozen (-80°C). Slices (thickness of 10 µm) were prepared using the cryotom (Leica CM1950) at -20°C and three slices of each tissue were applied to one object slide (diagnostic microsocope slides, ThermoFisher, X2XER203B).

The following buffer systems were used: assay buffer pH 7.4 (100 mM MOPS, 0 or 3 mM $CaCl_2$, 50 µM EDTA, 0 or 5 mM DTT, adjusted to pH 7.4 with 1 M NaOH) and PBS++ (Biochrom). Tissue/ tumour sections were immediately transferred to the assay buffer (pH 7.4, $CaCl_2$-free) and incubated for 10 min prior to the addition of the radiotracer solution. A 0.5 MBq/mL solution of [^{18}F]**7b** was prepared in the respective assay buffer. For blocking experiments, compound **7a** (10 µM) or **7b** (10 µM) was added to this solution. Incubation of the slices with the radiotracer solution (100 µL) was done for 1 h at 37 °C. Afterwards, the solution was removed and the object slides were washed three times with PBS++ and dried (10 min).

Radioactive regions were visualised by using the Amersham Typhoon 5 Biomolecular Imager. The radioluminograms were analysed by the software AIDA (Advanced Image Data Analyzer, version 5.1 SP4 Build 1244) using the 2D TLC evaluation mode. For quantification of the radioactive regions, a TLC stripe with spots of defined activity of [^{18}F]**7b** was placed under the same imaging plate as used for the object slides.

Associated Content

Supporting Information

All synthetic methods and analytical data (NMR, ESI-MS) of the compounds, further experimental descriptions and additional Figures and Schemes (as mentioned in the text) are included in the Supporting Information. (PDF)

Molecular Formular Strings (CSV)

Author Information

*E-mail: r.wodtke@hzdr.de; r.loeser@hzdr.de

Conflict of interest

There are no conflicts to declare.

Acknowledgments

We cordially appreciate the expert support of Catharina Knöfel, Mareike Barth, Annegret Riedel, Lydia Behring and Regina Herrlich in cell culture, organ/tumour preparation, and autoradiography experiments. The excellent technical assistance of Kay Fischer and Alan Wong in the organic synthesis is greatly acknowledged. The authors thank Stephan Preusche and Dr. Martin Kreller and the cyclotron team for providing [^{18}F]fluoride. Furthermore, we wish to thank Drs. Friedrich-Alexander Ludwig and Steffen Fischer for helpful discussions concerning autoradiography of tissue sections. The A375-hS100A4 cells were generated by our former colleague Dr. Nadine Herwig (née Tandler) as part of her doctoral thesis. Partial financial support by the Helmholtz Cross-Programme Initiative “Technology and Medicine – Adaptive Systems” (S.H., C.N., J.P.) and by the Fonds der Chemischen Industrie (R.L.) is gratefully acknowledged. Partial support of this work was provided to J.P. and C.N. within the Collaborative Research Center Transregio 67 “Functional biomaterials for controlling healing processes in bone and skin – from material science to clinical application” (TRR 67/3) by the Deutsche Forschungsgemeinschaft (DFG).

Abbreviations used

DAD, diode array detector; DIPEA, *N*,*N*-diisopropylethylamine; DMEM, Dulbecco's modified Eagle's medium; hTGase 2, human transglutaminase 2; PyBOP, benzotriazol-1-yloxytripyrrolidinophosphonium hexafluorophosphate; TCEP, tris(2-carboxyethyl)phosphine; TEA, triethylamine

References and Notes

1. Evans, M. J. and Cravatt, B. F. Mechanism-based profiling of enzyme families. *Chem. Rev.*, **2006**, *106*, 3279-3301.
2. Cravatt, B. F.; Wright, A. T. and Kozarich, J. W. Activity-based protein profiling: from enzyme chemistry to proteomic chemistry. *Annu. Rev. Biochem.*, **2008**, *77*, 383-414.
3. Heal, W. P.; Dang, T. H. and Tate, E. W. Activity-based probes: discovering new biology and new drug targets. *Chem. Soc. Rev.*, **2011**, *40*, 246-257.
4. Willems, L. I.; Overkleeft, H. S. and van Kasteren, S. I. Current developments in activity-based protein profiling. *Bioconjug. Chem.*, **2014**, *25*, 1181-1191.
5. Willems, L. I.; Jiang, J.; Li, K. Y.; Witte, M. D.; Kallemeijn, W. W.; Beenakker, T. J.; Schroder, S. P.; Aerts, J. M.; van der Marel, G. A.; Codee, J. D. and Overkleeft, H. S. From covalent glycosidase inhibitors to activity-based glycosidase probes. *Chem. Eur. J.*, **2014**, *20*, 10864-10872.
6. Qiu, H.; Caldwell, R.; Liu-Bujalski, L.; Goutopoulos, A.; Jones, R.; Potnick, J.; Sherer, B.; Bender, A.; Grenningloh, R.; Xu, D.; Gardberg, A.; Mochalkin, I.; Johnson, T.; Viacava Follis, A.; Head, J. and Morandi, F. Discovery of affinity-based probes for BTK occupancy assays. *ChemMedChem*, **2019**, *14*, 217-223.
7. van der Zouwen, A. J.; Lohse, J.; Wieske, L. H. E.; Hohmann, K. F.; van der Vlag, R. and Witte, M. D. An *in situ* combinatorial methodology to synthesize and screen chemical probes. *Chem. Commun.*, **2019**, *55*, 2050-2053.
8. Fonovic, M. and Bogyo, M. Activity-based probes as a tool for functional proteomic analysis of proteases. *Expert. Rev. Proteomics*, **2008**, *5*, 721-730.
9. Serim, S.; Haedke, U. and Verhelst, S. H. Activity-based probes for the study of proteases: recent advances and developments. *ChemMedChem*, **2012**, *7*, 1146-1159.
10. Jiang, J.; Kuo, C. L.; Wu, L.; Franke, C.; Kallemeijn, W. W.; Florea, B. I.; van Meel, E.; van der Marel, G. A.; Codee, J. D.; Boot, R. G.; Davies, G. J.; Overkleeft, H. S. and Aerts, J. M. Detection of active mammalian

GH31 α-glucosidases in health and disease using in-class, broad-spectrum activity-based probes. *ACS Cent. Sci.*, **2016**, *2*, 351-358.

11. Kreuzer, J.; Bach, N. C.; Forler, D. and Sieber, S. A. Target discovery of acivicin in cancer cells elucidates its mechanism of growth inhibition. *Chem. Sci.*, **2014**, *6*, 237-245.
12. Koenders, S. T. A.; Wijaya, L. S.; Erkelens, M. N.; Bakker, A. T.; van der Noord, V. E.; van Rooden, E. J.; Burggraaff, L.; Putter, P. C.; Botter, E.; Wals, K.; van den Elst, H.; den Dulk, H.; Florea, B. I.; van de Water, B.; van Westen, G. J. P.; Mebius, R. E.; Overkleeft, H. S.; Le Devedec, S. E. and van der Stelt, M. Development of a retinal-based probe for the profiling of retinaldehyde dehydrogenases in cancer cells. *ACS Cent. Sci.*, **2019**, *5*, 1965-1974.
13. Sacks, J. Radioactive isotopes as indicators in biology. *Chem. Rev.*, **1948**, *42*, 411-456.
14. Ostrowski, K. and Barnard, E. A. Application of isotopically-labelled specific inhibitors as a method in enzyme cytochemistry. *Exp. Cell Res.*, **1961**, *25*, 465-&.
15. Rogers, A. W.; Darzynkiewicz, Z.; Salpeter, M. M.; Ostrowski, K. and Barnard, E. A. Quantitative studies on enzymes in structures in striated muscles by labeled inhibitor methods. I. The number of acetylcholinesterase molecules and of other DFP-reactive sites at motor endplates, measured by radioautography. *J. Cell Biol.*, **1969**, *41*, 665-685.
16. Fenteany, G.; Standaert, R. F.; Lane, W. S.; Choi, S.; Corey, E. J. and Schreiber, S. L. Inhibition of proteasome activities and subunit-specific amino-terminal threonine modification by lactacystin. *Science*, **1995**, *268*, 726-731.
17. Kozarich, J. W. and Strominger, J. L. A membrane enzyme from *staphylococcus aureus* which catalyzes transpeptidase, carboxypeptidase, and penicillinase activities. *J. Biol. Chem.*, **1978**, *253*, 1272-1278.
18. Chambers, H. F. and Sachdeva, M. Binding of β-lactam antibiotics to penicillin-binding proteins in methicillin-resistant *staphylococcus aureus*. *J. Inf. Dis.*, **1990**, *161*, 1170-1176.
19. Preston, D. A.; Wu, C. Y.; Blaszczak, L. C.; Seitz, D. E. and Halligan, N. G. Biological characterization of a new radioactive labeling reagent for bacterial penicillin-binding proteins. *Antimicrob. Agents Chemother.*, **1990**, *34*, 718-721.
20. Bogyo, M.; Verhelst, S.; Bellingard-Dubouchaud, V.; Toba, S. and Greenbaum, D. Selective targeting of lysosomal cysteine proteases with radiolabeled electrophilic substrate analogs. *Chem. Biol.*, **2000**, *7*, 27-38.
21. Greenbaum, D.; Medzihradszky, K. F.; Burlingame, A. and Bogyo, M. Epoxide electrophiles as activity-dependent cysteine protease profiling and discovery tools. *Chem. Biol.*, **2000**, *7*, 569-581.
22. Borodovsky, A.; Ovaa, H.; Kolli, N.; Gan-Erdene, T.; Wilkinson, K. D.; Ploegh, H. L. and Kessler, B. M. Chemistry-based functional proteomics reveals novel members of the deubiquitinating enzyme family. *Chem. Biol.*, **2002**, *9*, 1149-1159.

23. Eckert, R. L. Transglutaminase 2 takes center stage as a cancer cell survival factor and therapy target. *Mol. Carcinog.*, **2019**, *58*, 837-853.

24. Benn, M. C.; Weber, W.; Klotzsch, E.; Vogel, V. and Pot, S. A. Tissue transglutaminase in fibrosis — more than an extracellular matrix cross-linker. *Curr. Op. Biomedical Engineer.*, **2019**, *10*, 156-164.

25. Szondy, Z.; Korponay-Szabo, I.; Kiraly, R.; Sarang, Z. and Tsay, G. J. Transglutaminase 2 in human diseases. *Biomedicine*, **2017**, *7*, 1-13.

26. Klöck, C.; DiRaimondo, T. R. and Khosla, C. Role of transglutaminase 2 in celiac disease pathogenesis. *Semin. Immunopathol.*, **2012**, *34*, 513-522.

27. Rauhavirta, T.; Hietikko, M.; Salmi, T. and Lindfors, K. Transglutaminase 2 and transglutaminase 2 autoantibodies in celiac disease: a review. *Clin. Rev. Allergy Immunol.*, **2019**, *57*, 23-38.

28. Kanchan, K.; Fuxreiter, M. and Fesus, L. Physiological, pathological, and structural implications of non-enzymatic protein-protein interactions of the multifunctional human transglutaminase 2. *Cell. Mol. Life Sci.*, **2015**, *72*, 3009-3035.

29. Katt, W. P.; Antonyak, M. A. and Cerione, R. A. Opening up about tissue transglutaminase: when conformation matters more than enzymatic activity. *Med. One*, **2018**, *3*, e180011.

30. Dafik, L. and Khosla, C. Dihydroisoxazole analogs for labeling and visualization of catalytically active transglutaminase 2. *Chem. Biol.*, **2011**, *18*, 58-66.

31. Adam, G. C.; Sorensen, E. J. and Cravatt, B. F. Trifunctional chemical probes for the consolidated detection and identification of enzyme activities from complex proteomes. *Mol. Cell. Proteomics*, **2002**, *1*, 828-835.

32. Keillor, J. W.; Clouthier, C. M.; Apperley, K. Y.; Akbar, A. and Mulani, A. Acyl transfer mechanisms of tissue transglutaminase. *Bioorg. Chem.*, **2014**, *57*, 186-197.

33. Marrano, C.; de Macédo, P. and Keillor, J. W. Evaluation of novel dipeptide-bound α,β-unsaturated amides and epoxides as irreversible inhibitors of guinea pig liver transglutaminase. *Bioorg. Med. Chem. Lett.*, **2001**, *9*, 1923-1928.

34. Wityak, J.; Prime, M. E.; Brookfield, F. A.; Courtney, S. M.; Erfan, S.; Johnsen, S.; Johnson, P. D.; Li, M.; Marston, R. W.; Reed, L.; Vaidya, D.; Schaertl, S.; Pedret-Dunn, A.; Beconi, M.; Macdonald, D.; Muñoz-Sanjuan, I. and Dominguez, C. SAR development of lysine-based irreversible inhibitors of transglutaminase 2 for huntington's disease. *ACS Med. Chem. Lett.*, **2012**, *3*, 1024-1028.

35. Akbar, A.; McNeil, N. M. R.; Albert, M. R.; Ta, V.; Adhikary, G.; Bourgeois, K.; Eckert, R. L. and Keillor, J. W. Structure-activity relationships of potent, targeted covalent inhibitors that abolish both the transamidation and GTP binding activities of human tissue transglutaminase. *J. Med. Chem.*, **2017**, *60*, 7910-7927.

36. Wodtke, R.; Hauser, C.; Ruiz-Gomez, G.; Jäckel, E.; Bauer, D.; Lohse, M.; Wong, A.; Pufe, J.; Ludwig, F. A.; Fischer, S.; Hauser, S.; Greif, D.; Pisabarro, M. T.; Pietzsch, J.; Pietsch, M. and Löser, R. *N*$^{\varepsilon}$-Acryloyllysine

piperazides as irreversible inhibitors of transglutaminase 2: synthesis, structure-activity relationships, and pharmacokinetic profiling. *J. Med. Chem.*, **2018**, *61*, 4528-4560.

37. Evans, E. K.; Tester, R.; Aslanian, S.; Karp, R.; Sheets, M.; Labenski, M. T.; Witowski, S. R.; Lounsbury, H.; Chaturvedi, P.; Mazdiyasni, H.; Zhu, Z.; Nacht, M.; Freed, M. I.; Petter, R. C.; Dubrovskiy, A.; Singh, J. and Westlin, W. F. Inhibition of Btk with CC-292 provides early pharmacodynamic assessment of activity in mice and humans. *J. Pharmacol. Exp. Ther.*, **2013**, *346*, 219-228.
38. Prevet, H. and Collins, I. Labelled chemical probes for demonstrating direct target engagement in living systems. *Future Med. Chem.*, **2019**, *11*, 1195-1224.
39. Stöcklin, G.; Qaim, S. M. and Rösch, F. The impact of radioactivity on medicine. *Radiochim. Acta*, **1995**, *70/71*, 249-272.
40. Edem, P. E.; Steen, E. J. L.; Kjær, A. and Herth, M. M., Fluorine-18 Radiolabeling Strategies—Advantages and Disadvantages of Currently Applied Labeling Methods. In *Late-Stage Fluorination of Bioactive Molecules and Biologically-Relevant Substrates*, ed. A. Postigo, Elsevier, Amsterdam, 2019, DOI: 10.1016/b978-0-12-812958-6.00002-1, pp. 29-103.
41. Ermert, J. and Neumaier, B., The Radiopharmaceutical Chemistry of Fluorine-18: Nucleophilic Fluorinations. In *Radiopharmaceutical Chemistry*, eds. J. S. Lewis, A. D. Windhorst and B. M. Zeglis, Springer Nature, Cham, 2019, DOI: 10.1007/978-3-319-98947-1_15, ch. Chapter 15, pp. 273-283.
42. Folk, J. E. and Cole, P. W. Identification of a functional cysteine essential for the activity of guinea pig liver transglutaminase. *J. Biol. Chem.*, **1966**, *241*, 3238-3240.
43. van der Wildt, B.; Wilhelmus, M. M.; Bijkerk, J.; Haveman, L. Y.; Kooijman, E. J.; Schuit, R. C.; Bol, J. G.; Jongenelen, C. A.; Lammertsma, A. A.; Drukarch, B. and Windhorst, A. D. Development of carbon-11 labeled acryl amides for selective PET imaging of active tissue transglutaminase. *Nucl. Med. Biol.*, **2016**, *43*, 232-242.
44. van der Wildt, B.; Wilhelmus, M. M.; Kooijman, E. J.; Jongenelen, C. A.; Schuit, R. C.; Büchold, C.; Pasternack, R.; Lammertsma, A. A.; Drukarch, B. and Windhorst, A. D. Development of fluorine-18 labeled peptidic PET tracers for imaging active tissue transglutaminase. *Nucl. Med. Biol.*, **2016**, *44*, 90-104.
45. van der Wildt, B.; Wilhelmus, M. M. M.; Beaino, W.; Kooijman, E. J. M.; Schuit, R. C.; Bol, J.; Breve, J. J. P.; Pasternack, R.; Lammertsma, A. A.; Windhorst, A. D. and Drukarch, B. In vivo evaluation of two tissue transglutaminase PET tracers in an orthotopic tumour xenograft model. *EJNMMI Res.*, **2018**, *8*, 39.
46. Richarz, R.; Krapf, P.; Zarrad, F.; Urusova, E. A.; Neumaier, B. and Zlatopolskiy, B. D. Neither azeotropic drying, nor base nor other additives: a minimalist approach to ^{18}F-labeling. *Org. Biomol. Chem.*, **2014**, *12*, 8094-8099.
47. Yin, J. and Buchwald, S. L. Palladium-catalyzed intermolecular coupling of aryl halides and amides. *Org. Lett.*, **2000**, *2*, 1101-1104.

48. Hauser, C.; Wodtke, R.; Löser, R. and Pietsch, M. A fluorescence anisotropy-based assay for determining the activity of tissue transglutaminase. *Amino Acids*, **2017**, *49*, 567-583.

49. Flanagan, M. E.; Abramite, J. A.; Anderson, D. P.; Aulabaugh, A.; Dahal, U. P.; Gilbert, A. M.; Li, C.; Montgomery, J.; Oppenheimer, S. R.; Ryder, T.; Schuff, B. P.; Uccello, D. P.; Walker, G. S.; Wu, Y.; Brown, M. F.; Chen, J. M.; Hayward, M. M.; Noe, M. C.; Obach, R. S.; Philippe, L.; Shanmugasundaram, V.; Shapiro, M. J.; Starr, J.; Stroh, J. and Che, Y. Chemical and computational methods for the characterization of covalent reactive groups for the prospective design of irreversible inhibitors. *J. Med. Chem.*, **2014**, *57*, 10072-10079.

50. Jackson, P. A.; Widen, J. C.; Harki, D. A. and Brummond, K. M. Covalent modifiers: a chemical perspective on the reactivity of α,β-unsaturated carbonyls with thiols via hetero-Michael addition reactions. *J. Med. Chem.*, **2017**, *60*, 839-885.

51. Radio-TLC means autoradiography of thin layer plates after chromatographic separation using the phosphorimaging technique as detection method.

52. McDonald, A. G. and Tipton, K. F., Enzymes: Irreversible Inhibition. In *eLS (Ed.)*, John Wiley & Sons, Chichester, 2012, pp. 1-17.

53. Miyahisa, I.; Sameshima, T. and Hixon, M. S. Rapid determination of the specificity constant of irreversible inhibitors (k_{inact}/K_I) by means of an endpoint competition assay. *Angew. Chem. Int. Ed. Engl.*, **2015**, *54*, 14099-14102.

54. Wodtke, R.; Schramm, G.; Pietzsch, J.; Pietsch, M. and Löser, R. Synthesis and kinetic characterisation of water-soluble fluorogenic acyl donors for transglutaminase 2. *ChemBioChem*, **2016**, *17*, 1263-1281.

55. Basso, M. and Ratan, R. R. Transglutaminase is a therapeutic target for oxidative stress, excitotoxicity and stroke: a new epigenetic kid on the CNS block. *J. Cereb. Blood Flow Metab.*, **2013**, *33*, 809-818.

56. Lorand, L. and Conrad, S. M. Transglutaminases. *Mol Cell Biochem*, **1984**, *58*, 9-35.

57. Case, A.; Ni, J.; Yeh, L. A. and Stein, R. L. Development of a mechanism-based assay for tissue transglutaminase--results of a high-throughput screen and discovery of inhibitors. *Anal. Biochem.*, **2005**, *338*, 237-244.

58. Bergamini, C. M. GTP modulates calcium binding and cation-induced conformational changes in erythrocyte transglutaminase. *FEBS Lett.*, **1988**, *239*, 255-258.

59. Kiraly, R.; Csosz, E.; Kurtan, T.; Antus, S.; Szigeti, K.; Simon-Vecsei, Z.; Korponay-Szabo, I. R.; Keresztessy, Z. and Fesüs, L. Functional significance of five noncanonical Ca^{2+}-binding sites of human transglutaminase 2 characterized by site-directed mutagenesis. *FEBS J.*, **2009**, *276*, 7083-7096.

60. Clouthier, C. M.; Mironov, G. G.; Okhonin, V.; Berezovski, M. V. and Keillor, J. W. Real-time monitoring of protein conformational dynamics in solution using kinetic capillary electrophoresis. *Angew. Chem. Int. Ed.*, **2012**, *51*, 12464-12468.

61. Mironov, G. G.; Clouthier, C. M.; Akbar, A.; Keillor, J. W. and Berezovski, M. V. Simultaneous analysis of enzyme structure and activity by kinetic capillary electrophoresis-MS. *Nat. Chem. Biol.*, **2016**, *12*, 918-922.

62. Caron, N. S.; Munsie, L. N.; Keillor, J. W. and Truant, R. Using FLIM-FRET to measure conformational changes of transglutaminase type 2 in live cells. *PLOS ONE*, **2012**, *7*, e44159.

63. Achyuthan, K. E. and Greenberg, C. S. Identification of a guanosine triphosphate-binding site on guinea pig liver transglutaminase. Role of GTP and calcium ions in modulating activity. *J. Biol. Chem.*, **1987**, *262*, 1901-1906.

64. Begg, G. E.; Carrington, L.; Stokes, P. H.; Matthews, J. M.; Wouters, M. A.; Husain, A.; Lorand, L.; Iismaa, S. E. and Graham, R. M. Mechanism of allosteric regulation of transglutaminase 2 by GTP. *Proc. Natl. Acad. Sci. U.S.A*, **2006**, *103*, 19683-19688.

65. Schaertl, S.; Prime, M.; Wityak, J.; Dominguez, C.; Munoz-Sanjuan, I.; Pacifici, R. E.; Courtney, S.; Scheel, A. and Macdonald, D. A profiling platform for the characterization of transglutaminase 2 (TG2) inhibitors. *J. Biomol. Screen.*, **2010**, *15*, 478-487.

66. Harris, T. K. and Turner, G. J. Structural basis of perturbed pK_a values of catalytic groups in enzyme active sites. *IUBMB life*, **2002**, *53*, 85-98.

67. Radio-SDS-PAGE means autoradiography of a polyacrylamide gel after electrophoretic separation using the phosphorimaging technique as detection method.

68. Kim, N.; Lee, W. K.; Lee, S. H.; Jin, K. S.; Kim, K. H.; Lee, Y.; Song, M. and Kim, S. Y. Inter-molecular crosslinking activity is engendered by the dimeric form of transglutaminase 2. *Amino Acids*, **2016**, DOI: 10.1007/s00726-016-2293-1.

69. Stamnaes, J.; Iversen, R.; du Pre, M. F.; Chen, X. and Sollid, L. M. Enhanced B-cell receptor recognition of the autoantigen transglutaminase 2 by efficient catalytic self-multimerization. *PLoS One*, **2015**, *10*, e0134922.

70. The TGase 2 amount which can be activated under artifical conditions (high Ca^{2+}/DTT concentration) is herein after reffered to activatable TGase 2. This amount of activatable TGase 2 represents neither the amount of TGase 2 active under physiological conditions nor necessarily the total protein amount.

71. Wang, Z. and Griffin, M. The role of TG2 in regulating S100A4-mediated mammary tumour cell migration. *PLOS ONE*, **2013**, *8*, e57017.

72. Biri, B.; Kiss, B.; Kiraly, R.; Schlosser, G.; Lang, O.; Kohidai, L.; Fesus, L. and Nyitray, L. Metastasis-associated S100A4 is a specific amine donor and an activity-independent binding partner of transglutaminase-2. *Biochem. J.*, **2016**, *473*, 31-42.

73. Tandler, N.; Mosch, B. and Pietzsch, J. Protein and non-protein biomarkers in melanoma: a critical update. *Amino Acids*, **2012**, *43*, 2203-2230.

74. Zhang, J.; Lesort, M.; Guttmann, R. P. and Johnson, G. V. Modulation of the *in situ* activity of tissue transglutaminase by calcium and GTP. *J. Biol. Chem.*, **1998**, *273*, 2288-2295.

75. Gundemir, S. and Johnson, G. V. Intracellular localization and conformational state of transglutaminase 2: implications for cell death. *PLoS One*, **2009**, *4*, e6123.

76. Caputo, I.; Secondo, A.; Lepretti, M.; Paolella, G.; Auricchio, S.; Barone, M. V. and Esposito, C. Gliadin peptides induce tissue transglutaminase activation and ER-stress through Ca^{2+} mobilization in Caco-2 cells. *PLoS One*, **2012**, *7*, e45209.

77. Rossin, F.; D'Eletto, M.; Falasca, L.; Sepe, S.; Cocco, S.; Fimia, G. M.; Campanella, M.; Mastroberardino, P. G.; Farrace, M. G. and Piacentini, M. Transglutaminase 2 ablation leads to mitophagy impairment associated with a metabolic shift towards aerobic glycolysis. *Cell Death Differ.*, **2015**, *22*, 408-418.

78. D'Eletto, M.; Farrace, M. G.; Rossin, F.; Strappazzon, F.; Giacomo, G. D.; Cecconi, F.; Melino, G.; Sepe, S.; Moreno, S.; Fimia, G. M.; Falasca, L.; Nardacci, R. and Piacentini, M. Type 2 transglutaminase is involved in the autophagy-dependent clearance of ubiquitinated proteins. *Cell Death Differ.*, **2012**, *19*, 1228-1238.

79. D'Eletto, M.; Rossin, F.; Occhigrossi, L.; Farrace, M. G.; Faccenda, D.; Desai, R.; Marchi, S.; Refolo, G.; Falasca, L.; Antonioli, M.; Ciccosanti, F.; Fimia, G. M.; Pinton, P.; Campanella, M. and Piacentini, M. Transglutaminase type 2 regulates ER-mitochondria contact sites by interacting with GRP75. *Cell Rep.*, **2018**, *25*, 3573-3581 e3574.

80. Katt, W. P.; Antonyak, M. A. and Cerione, R. A. Simultaneously targeting tissue transglutaminase and kidney type glutaminase sensitizes cancer cells to acid toxicity and offers new opportunities for therapeutic intervention. *Mol. Pharm.*, **2015**, *12*, 46-55.

81. Biau, J.; Chautard, E.; Court, F.; Pereira, B.; Verrelle, P.; Devun, F.; De Koning, L. and Dutreix, M. Global conservation of protein status between cell lines and xenografts. *Transl. Oncol.*, **2016**, *9*, 313-321.

82. Soveg, F.; Abdala-Valencia, H.; Campbell, J.; Morales-Nebreda, L.; Mutlu, G. M. and Cook-Mills, J. M. Regulation of allergic lung inflammation by endothelial cell transglutaminase 2. *Am. J. Physiol. Lung Cell. Mol. Physiol.*, **2015**, *309*, L573-583.

83. Sun, H. and Kaartinen, M. T. Transglutaminase activity regulates differentiation, migration and fusion of osteoclasts via affecting actin dynamics. *J. Cell. Physiol.*, **2018**, *233*, 7497-7513.

84. Euhus, D. M.; Hudd, C.; LaRegina, M. C. and Johnson, F. E. Tumor measurement in the nude mouse. *J. Surg. Oncol.*, **1986**, *31*, 229-234.

85. (C) 2011 Allen Institute for Brain Science. Allen Mouse Brain Atlas. Available from: http://mouse.brain-map.org/).

86. Rudlong, J.; Cheng, A. and Johnson, G. V. W. The role of transglutaminase 2 in mediating glial cell function and pathophysiology in the central nervous system. *Anal. Biochem.*, **2020**, *591*, 113556.

87. Fukui, M.; Kuramoto, K.; Yamasaki, R.; Shimizu, Y.; Itoh, M.; Kawamoto, T. and Hitomi, K. Identification of a highly reactive substrate peptide for transglutaminase 6 and its use in detecting transglutaminase activity in the skin epidermis. *FEBS J.*, **2013**, *280*, 1420-1429.

88. Itoh, M.; Kawamoto, T.; Tatsukawa, H.; Kojima, S.; Yamanishi, K. and Hitomi, K. *In situ* detection of active transglutaminases for keratinocyte type (TGase 1) and tissue type (TGase 2) using fluorescence-labeled highly reactive substrate peptides. *J. Histochem. Cytochem.*, **2011**, *59*, 180-187.

89. Waters, J. C. Accuracy and precision in quantitative fluorescence microscopy. *J Cell Biol*, **2009**, *185*, 1135-1148.

90. Poreba, M.; Groborz, K. M.; Rut, W.; Pore, M.; Snipas, S. J.; Vizovisek, M.; Turk, B.; Kuhn, P.; Drag, M. and Salvesen, G. S. Multiplexed probing of proteolytic enzymes using mass cytometry-compatible activity-based probes. *J. Am. Chem. Soc.*, **2020**, *142*, 16704-16715.

91. Herwig, N.; Belter, B.; Wolf, S.; Haase-Kohn, C. and Pietzsch, J. Interaction of extracellular S100A4 with RAGE prompts prometastatic activation of A375 melanoma cells. *J. Cell Mol. Med.*, **2016**, *20*, 825-835.

92. Gassner, C.; Neuber, C.; Laube, M.; Bergmann, R.; Kniess, T. and Pietzsch, J. Development of a ^{18}F-labeled diaryl-substituted dihydropyrrolo[3,2,1-*hi*]indole as potential probe for functional imaging of cyclooxygenase-2 with PET. *ChemistrySelect*, **2016**, *1*, 5812-5820.

93. Neuber, C.; Belter, B.; Meister, S.; Hofheinz, F.; Bergmann, R.; Pietzsch, H. J. and Pietzsch, J. Overexpression of receptor tyrosine kinase EphB4 triggers tumor growth and hypoxia in A375 melanoma xenografts: insights from multitracer small animal imaging experiments. *Molecules*, **2018**, *23*.

Table of Contents Graphic

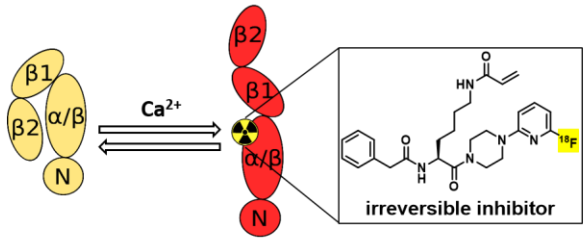

*Quantitative detection of **active transglutaminase 2** by autoradiography*